IOWA STATE UNIVERSITY
Digital Repository

2009

An experimental study of the vortex structures in the wake of a piezoelectric flapping plate for Nano Air Vehicle applications

Lucas Clemons
Iowa State University

Follow this and additional works at: https://lib.dr.iastate.edu/etd

 Part of the Aerospace Engineering Commons

An experimental study of the vortex structures in the wake of a piezoelectric flapping plate

for Nano Air Vehicle applications

by

Lucas A. Clemons

A thesis submitted to the graduate faculty

in partial fulfillment of the requirements for the degree of

MASTER OF SCIENCE

Major: Aerospace Engineering

Program of Study Committee:
Hui Hu, Major Professor
Tom Shih
Terrence Meyer

Iowa State University

Ames, Iowa

2009

TABLE OF CONTENTS

LIST OF FIGURES

LIST OF TABLES

NOMENCLATURE

AoA	Angle of Attack
UAV	Unmanned Air Vehicle
MAV	Micro-Air Vehicle
NAV	Nano-Air Vehicle
PIV	Particle Image Velocimetry
J	Advance Ratio
k	Reduced Frequency
St	Strouhal Number
f	Flapping Frequency
A	Peak to Peak Flapping Amplitude
V_∞	Free-Stream Velocity
h	Non-Dimensional Amplitude
kh	Non-Dimensional Velocity
c	Chord Length

ABSTRACT

The purpose of the current study is to verify the vortex wake structure results of a flapping piezoelectric plate with the heaving airfoils of previous studies and then explore at low Reynolds numbers (<15000, the designated flight domain of Nano Air Vehicles) how the vortex wake structure depends on advance ratio, angle of attack, flapping amplitude, and by span-wise location on the piezoelectric flapping plate. Using Particle Image Velocimetry, a non-intrusive optical measurement technique, the two dimensional velocity, turbulent kinetic energy, and vorticity information was obtained to better understand the flight regime of unsteady flapping flight. As previously shown in works such as Lai and Platzer (1999), unsteady flapping flight conditions, advance ratio below unity, produces vortex wake structures that generate thrust and increasing advance ratio reduces this benefit. Increasing advance ratio obtained by varying incoming flow velocity or the flapping amplitude was compared by vortex structure as well as the thrust generated by flapping, which was found to decrease more rapidly with decreasing the flapping amplitude. The effect of changing the flapping amplitude has an effect on both the wake structure type and size. Increasing angle of attack causes greatly increased drag but did not significantly change the vortex structure type seen for the angles of attack used in this experiment. The effect of span-wise location was found to be independent of the decreased flapping amplitude and understanding the phenomenon demands further study.

CHAPTER 1. OVERVIEW

As the size of unmanned aerial vehicles (MAVs) become smaller and smaller the need to understand the underlying physics of flapping flight increases because of the interest of mimicking natural fliers as they share the same dimensions and flight capabilities desirable in certain MAV applications. The study presented here explores the vortex wake structures of a flapping plate to better understand how the thrust generated changes with varying free stream velocity (flight speed), span-wise location on the piezoelectric plate, flapping amplitude, and angle of attack conditions.

Introduction

The evolution of powered flight since the Wright brother first flew in 1905 has taken human pilots to fly at greater speeds and reach greater altitudes. Nature's fliers, such as birds and insects, were the inspiration for many early attempts at human flight but it was found that fixed wing aircraft were much more practical for that purpose. Today the flight regimes of nature's fliers are getting a second look because of the success of unmanned aerial vehicles, which are the greatest growth sector in today's aerospace industry. Current UAVs that are well known to the public, such as the Global Hawk and Predator Drone, are large aircraft on the same macro-scale as manned aircraft. These fixed wing aircraft are primarily used for surveillance but can also be used to carry out attack missions. An interest in making unmanned systems even smaller, such as micro-air vehicles (MAVs) and nano-air vehicles (NAVs) for such missions as indoor or urban surveillance, targeting, and life or biochemical

sensing in remote or dangerous locations, have generated interest in studying the physics of bird and insect flight for use in the development of new novel and efficient MAV designs. MAVs can be loosely defined as an air vehicle with a wingspan of less than 15 cm and capable of flight speeds less than 10 m/s. DARPA's NAV project defines an NAV as smaller than 7.5 cm and flies at Reynolds numbers < 15,000. These are the flight conditions that the current study has in interest. Because of their size, low flight speeds, and the maneuverability required for NAV missions (such as indoor obstacle avoidance) a traditional fixed wing approach is unable to provide the desired design characteristics. One possible approach is a flapping flight design that mimics the success of natural fliers.

Flapping Flight

To characterize the flapping flight for the current study the Advance Ratio was used as the fundamental parameter. The Advance Ratio (J) is a non-dimensional number defined as

$$J = \frac{V_\infty}{2Af}$$

where A is the peak to peak amplitude of the wingtip, f is the frequency of flapping, and V_∞ is the flight speed (or incoming flow velocity in a wind-tunnel experiment.) Therefore J is the ratio of the flight velocity to the wingtip velocity. By definition flapping flight is quasi steady for J > 1 and unsteady for J < 1. The figure below shows chord length c, A, and V_∞ on the front and side views of the piezoelectric plate used in the present study.
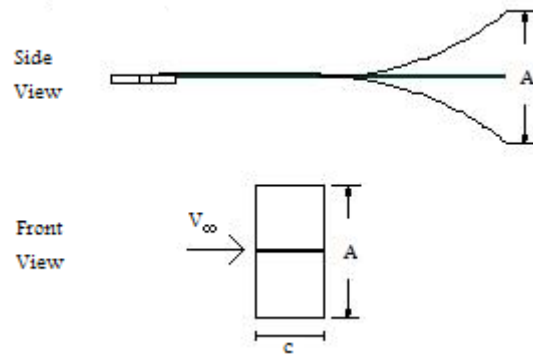
Figure 1. Front and Side Views of the Piezoelectric Plate

Large birds that soar, flapping their wings little during flight, behave closer to fixed wing flight putting them in the quasi steady flapping flight regime. Many of the previous works, such as Lai and Platzer (1999) and Young and Lai (2004), studying vortex sheet thrust generation of oscillating airfoils haven been in this region due to the higher Reynolds numbers used in those studies. In these studies the oscillating airfoil is making a heaving motion which we compare to the wingtip of a flapping plate. In the present study a piezoelectric fan, essentially a flat plate that deforms when a voltage is passed through it that causes the material to 'flap,' was used and the fan tip is treated as the wingtip for purposes of defining the advance ratio. The focus of this study was to compare this work with previous studies and then expand by studying unsteady flapping flight. Unsteady flapping flight is the flight regime of small birds and insects and tends to be at lower Reynolds numbers than quasi-steady flapping flight. The unsteady flapping flight regime of insects, who fly at J= 0.3-0.6 and at Reynolds numbers of roughly 100-10,000, which puts them into the realm of Nano Air Vehicles (NAVs), is of interest in the current study.

The Advance Ratio is not the only parameter used to characterize flapping flight. The heaving airfoil studies above have made use of the reduced frequency, defined as

$$k = \frac{2\pi f c}{2V_\infty}$$

where f is the flapping frequency, c is the chord length, and V_∞ is the incoming flow velocity. Together with the non-dimensional amplitude h, defined as

$$h = \frac{A/2}{c}$$

gives us the non-dimensional velocity kh which can be related to J by

$$kh = \frac{\pi}{4J}$$

which this study will use to compare with previous studies. Finally the Strouhal number has also been used to characterize oscillating airfoil such as in Lua, ET AL (2007.) This is defined as

$$St = \frac{f\frac{A}{2}}{V_\infty} = \frac{1}{4J}$$

and it is simply the inverse of four times the Advance Ratio.

It has been shown in previous studies that a heaving or flapping airfoil can generate thrust depending on the conditions. The trailing edge wake structure of a flapping airfoil can indicate whether the flapping airfoil is producing drag or thrust. A von Kármán vortex sheet wake structure indicates a drag wake and a reverse von Kármán vortex sheet wake structure indicates thrust. A drag wake is typically characterized as pairs of vortices with the upper as clockwise and the lower as counter-clockwise forming a mushroom-like structure tilted

upstream to the free-stream flow direction. A thrust wake is a jet-like wake that is typically

characterized as pairs of vortices with the upper as counter-clockwise and the lower

clockwise forming a mushroom-like structure tilted downstream. A neutral wake structure is

characterized as multiple vortices shed per half-cycle whose vortex pairs are not tilted. This

is illustrated in the figure taken from Young and Lai (2004) shown below.
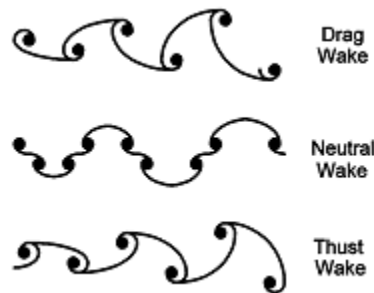
Figure 2. Illustration of Vortex Wake Structures from Young and Lai (2004)

These wake structures were shown to vary with J, where as J is decreasing the wake

structure goes from drag wake, to neutral wake, and finally to a thrust producing jet-like

wake. Young and Lai (2004) also suggested that there was some dependence on k and h on

the vortex structure. For the piezoelectric flapping plate used in the current study, at what J

the changes in vortex structure occur and whether the vortex structure has dependence on

other parameters in addition to J, such as h, AoA, or span-wise location, will be explored.

To indicate whether thrust or drag was being generated at a given condition a simple

method of indicating the strength of the forces in the x direction using the measured

velocities was used. Derived from the integral form of the momentum equation, the velocity

profiles ahead of the airfoil and two cord lengths behind the trailing edge of the airfoil were

used and the difference in area between them indicate whether additional velocity (indicating

thrust) was created by the flapping motion of the airfoil. The equation used is found below.

$$C_f = \frac{2}{c}\int(\frac{U_0}{U_\infty}(\frac{U_0}{U_\infty}-1))dy$$

In Figure 3 found below, the locations of the velocity profiles used to find the force

coefficient in the x-direction are shown relative to the wingtip cord location of the

piezoelectric airfoil.

U_∞ $\qquad\qquad\qquad\qquad\qquad\qquad\qquad\qquad\qquad\qquad\qquad$ U_0

piezoelectric plate

Figure 3. Location of Velocity Profiles used in Calculating Force Coefficient in x-Direction

Objectives

The objectives of this thesis are to:

- relate the work done here to previous results in the literature;

- determine the effect of changing advance ratio, angle of attack, flapping amplitude, and span-wise location on the vortex structure in the wake of the piezoelectric flapping plate;

Outline of the Thesis

To meet the stated objectives the thesis' further chapters present the information as follows:

In Chapter 2 a brief review of the literature is presented.

In Chapter 3 the experimental techniques and setup used are presented.

In Chapter 4 experimental results are presented.

In Chapter 5 the conclusions and recommendations of the Thesis are presented.

CHAPTER 2. REVIEW OF LITERATURE

Several past works have looking into the vortex wake structure of plunging or flapping airfoils and try to use this to predict the thrust. Most of these studies have been in the quasi-steady flapping flight regime and to the authors best knowledge this has been no work to quantitatively measure at low Reynolds numbers (< 10,000) in the unsteady-flapping flight regime how changes in J, flapping amplitude, span-wise location, and AoA effect vortex structure and thrust generation.

Introduction

Flapping flight in nature is a very complex phenomenon and yet it is found in numerous species of birds, insects, and bats. The study of these animal's ability to fly is often approached from a biological perspective. As studies into flapping flight for MAVs and NAVs are interested in the underlying physics of flapping flight these are approached by studying an aspect of flapping flight rather than studying exact flight mechanics of one species of animal. This is the case in the following studies.

Previous Studies

In the experimental work done by Lai and Platzer (1999) and the numerical work done by Young and Lai (2004), the researchers have studied oscillating two dimensional airfoils through the use of a heaving (plunging) airfoil. These works are important to the current study as they visualize and characterize the wake structures found behind heaving

airfoils and show that this type of motion can result in thrust production. The current study looks to relate its results to these results of a heaving airfoil.

Lai and Platzer's experimental work used flow visualization in a water tunnel to show how the vortex pattern changed in the wake of a heaving 2-D NACA 0012 airfoil with respect to the non-dimensional velocity kh. For example, at a chord Re of 20,000 with a constant frequency of 2.5 Hz and free-stream velocity of 0.2 m/s while varying h their results were as follows.

Table 1. Flow Visualization Results from Lai and Platzer's Heaving Airfoil

Lai and Platzer						
A (m)	H	kh	Strouhal	J	Re	Wake Structure
0.003	0.013	0.098	0.031	8.01	20000	Drag
0.005	0.025	0.196	0.062	4.01	20000	Neutral
0.01	0.050	0.393	0.125	2.00	20000	Thrust
0.015	0.075	0.589	0.187	1.33	20000	Thrust
0.02	0.100	0.785	0.250	1.00	20000	Thrust

Also they showed that by increasing the amplitude and decreasing the frequency while maintaining constant kh, for the thrust generating conditions, would give the same vortex structures but with smaller vortices showing that there is some dependence on not only J alone. Changing the frequency from 2.5 Hz to 5 Hz gave similar results in vortex structure at the same kh while the size of the vortices and their spacing apart from one another decreased. However upon increasing the frequency to 10 Hz, at the same kh as before, the vortices in the vortex sheet were even smaller and had much less distance between vortex centers and the structure was tilted more downstream. This downstream tilt is indicative of a thrust generating jet like vortex wake structure.

The numerical work of Young and Lai (2004) further showed this by using a Navier-Strokes solver to computationally recreate the results of Lai and Platzer (1999) and also

showed that the vortex wake structure is not dependant on kh alone. Using the same values of Re, h, and k from Lai and Platzer, this work showed good agreement between the experimental and the laminar numerical results. Using this good agreement as a measure of confidence in the physicality of their results, the researchers used their code to show how the wake structure of a von Kármán vortex sheet evolved with changing k and h while maintaining a constant kh. They found that reducing the frequency (and thereby increasing the amplitude) led to a more complex multiple vortex-per-half-cycle-type shedding from the simple von Kármán type wake structure found at the higher frequency.

Another interesting heaving airfoil experimental study by Lua ET AL (2007) was prompted by the numerical simulations of Lewin and Haj-Hariri (2003) and how they contrasted with the results of Lai and Platzer (1999.) The previous work had shown that the trailing edge generated the wake structures while Lewin and Haj-Hariri showed the structure depended on the leading edge and trailing edge vortex interaction. Lua ET AL experiments were done to verify Lewin and Haj-Hariri's work experimentally. These experiments were conducted in a water tunnel with a 20 mm chord length elliptic airfoil at a Re of 1000 with a free-stream velocity of 0.05 m/s and a heaving frequency from 0.25 to 2.5 Hz. Because of the large changes of amplitude and frequency while maintaining the same J the researchers showed again that the wake structure is not alone due to changes in J but to also to the amplitude and how that effects the leading and trailing edge vortices creation and interaction.

Table 2. Experimental Results of Lua ET AL

Lua, et al						
A (m)	H	kh	Strouhal	J	Re	Wake Structure
0.005	0.123	0.289	0.092	2.72	1000	Drag
0.007	0.184	0.289	0.092	2.72	1000	Thrust
0.006	0.160	0.503	0.160	1.56	1000	Thrust
0.013	0.320	0.503	0.160	1.56	1000	Neutral
0.064	1.600	0.503	0.160	1.56	1000	Neutral
0.011	0.276	0.867	0.276	0.91	1000	Thrust
0.015	0.368	0.867	0.276	0.91	1000	Thrust
0.022	0.552	0.867	0.276	0.91	1000	Thrust
0.044	1.104	0.867	0.276	0.91	1000	Thrust

Lua ET AL's study is of interest to the current research because of the similar Re and the fact it investigates an advance ratio less than one near the transition between quasi-steady and unsteady flapping flight. Lua ET AL concluded that the higher frequencies and smaller heaving amplitudes along with the airfoil shape resulted in Lai and Platzer's experiment to have less effect from the leading edge vortices. Of note is that in the current study the amplitudes are similar to those used in Lai and Platzer and a much higher flapping frequency is used than any tested by either of the previous experimental works.

CHAPTER 3. EXPERIMENTAL TECHINQUES AND SETUP

This chapter is divided into the following three parts: Particle Image Velocity (PIV), the method used for data acquisition, is discussed. An explanation of the experimental setup, wind-tunnel low speed velocity characterization, and piezo fan measurements and testing follows. Lastly the experimental design is outlined.

Particle Image Velocimetry

Particle Image Velocimetry (PIV) is a non-intrusive flow field measurement technique to acquire quantitative velocity field information. In PIV the free stream velocity is seeded with small particles. When air is the working fluid often oil based smoke particles are used as they are in the current study. A Corona Integrated Technologies Inc. Colt 4 was used to generate the smoke particles with diameters between 1-5μm. Behind PIV is an assumption that because of their small size the seed particles faithfully follow the flow. A laser beam, generated in this case by a NewWave Gemini 200 Nd:Yag laser at a wavelength of 532nm, is focused through a set of optics including a sheet generator resulting in a laser sheet of one millimeter thickness that can be used to illuminate a plane of interest. This plane of interest can be changed by adjusting the laser sheet's location through the use of mirrors. In the present study the wingtip location, parallel to the chord and perpendicular to the span-wise direction at a non-flapping zero AoA condition was our primary measurement plane. This location was adjusted span-wise to see the resulting effect on the vortex structure. A CCD camera can be synchronized to the laser firing so that the illuminated seed

particles are captured in an image as they follow the flow around the airfoil. In the present study the Cooke Corp Pixelfly CCD camera was used at a resolution of 1392x1024 pixels and the system was synchronized using a Berkley Nucleonics model 565 digital delay generator. By taking two such images within a known small time distance, Δt, a PIV image pair results. After using the Camware© computer software to record a set of images onto the host computer, the Insight© software was used locate the same particle in each image of an images pair and the distance and direction traveled can be determined over the known time period Δt. The result is a velocity vector field that after being processed by a C++ code developed by our lab that removes bad vectors the vorticity, turbulent kinetic energy, and mean-velocity information is obtained.

Setup and Initial Testing

Iowa State's low-speed blue research wind-tunnel was used in the present study to provide the free-stream velocity into which the piezo electric flapping plate is mounted. The wind-tunnel is closed circuit and can provide free-stream velocities as high as 50 m/s. The test section is optically clear with a foot square cross-section.

The Piezo Systems Inc. 115VAC/60Hz piezo fan blade was used as our flapping airfoil in this study. The piezoelectric element used is a ceramic that is non conductive, like all piezoelectric materials. When a voltage is passed into a piezoelectric material a proportional mechanical stress is created and vise-versa. Using this material property the piezoelectric plate deforms in a flapping motion to an alternating current power source that is at a frequency of 60 Hz, the resonance frequency of the material, and at an amplitude

dependant on the voltage applied. This piezoelectric plate could be driven directly off the AC power bus which would cause the piezo element to oscillate at 60 Hz and at consistent amplitude. In the present study a function generator (Gw Instek GFG-3015) set to a sin wave function and high voltage power amplifier (Trek Model 609E-6) monitored by an oscilloscope were used to drive the fan which allowed for control over the fan's amplitude by adjusting the voltage. Below the dimensions of the piezoelectric fan are given.
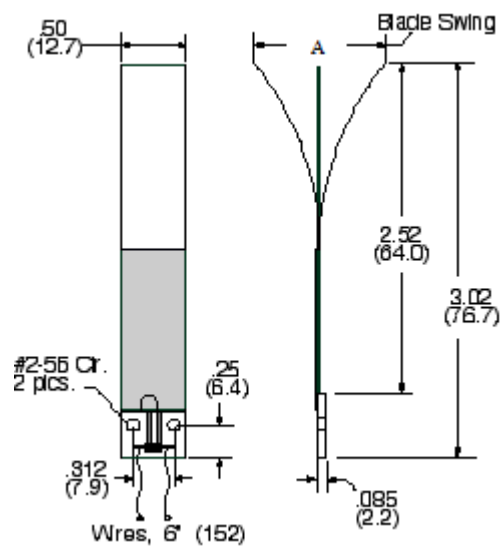
Figure 4. Dimensions of Piezo Systems 115VAC/60Hz Piezo Fan

The piezoelectric plate could be kept at a known, constant wingtip velocity for a given experiment and the desired advance ratio would be achieved by adjusting the flow speed in the wind-tunnel. The amplitude could also be adjusted while maintaining constant wind-tunnel flow to change the advance ratio. The resonance frequency of the piezo fan of 60Hz necessitated using one flapping frequency as the flapping amplitude rapidly decreases as the frequency moves away from 60 Hz. Despite the limitations in being unable to change the flapping frequency the piezoelectric plate has many advantages over the airfoils used in

the previous studies of Lai and Platzer (1999) and Lua ET AL (2007.) Their mechanically

driven airfoil heaving mechanisms were limited to much lower flapping frequencies (10 Hz

or under) and their non-dimensional flapping amplitudes (h) were also much smaller. Not

only does the piezoelectric plate k and h values better represent the natural flapping flyers

who's flight regime is the inspiration for the studying of flapping airfoils for NAVs but also

the three dimensional flapping motion of the piezoelectric flat plate more closely mimics

nature than the two dimensional heaving motion used in Lai and Platzer (1999) or in Lua ET

AL (2007.) The illustration found below in Figure 5 shows how the sin wave the function

generator uses to power the piezoelectric plate deforms the piezo element by phase angle.
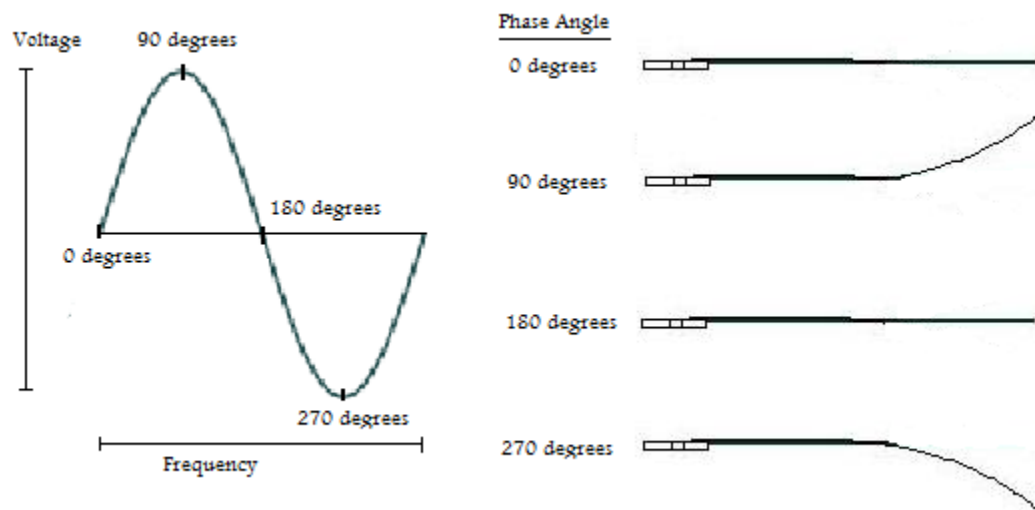
Figure 5. Illustration of Piezoelectric Plate Position by Sin Wave Phase Angle

The accuracy of the phase-lock is demonstrated below in Figure 6 that shows the

positions of the wingtip by phase angle plotted over a Sine curve. As can be seen the results

fit a symmetric sine wave.

Wingtip Position Versus Phase Angle on a Sine Wave for 3 Hz Wind-Tunnel Speed AoA 0 Case
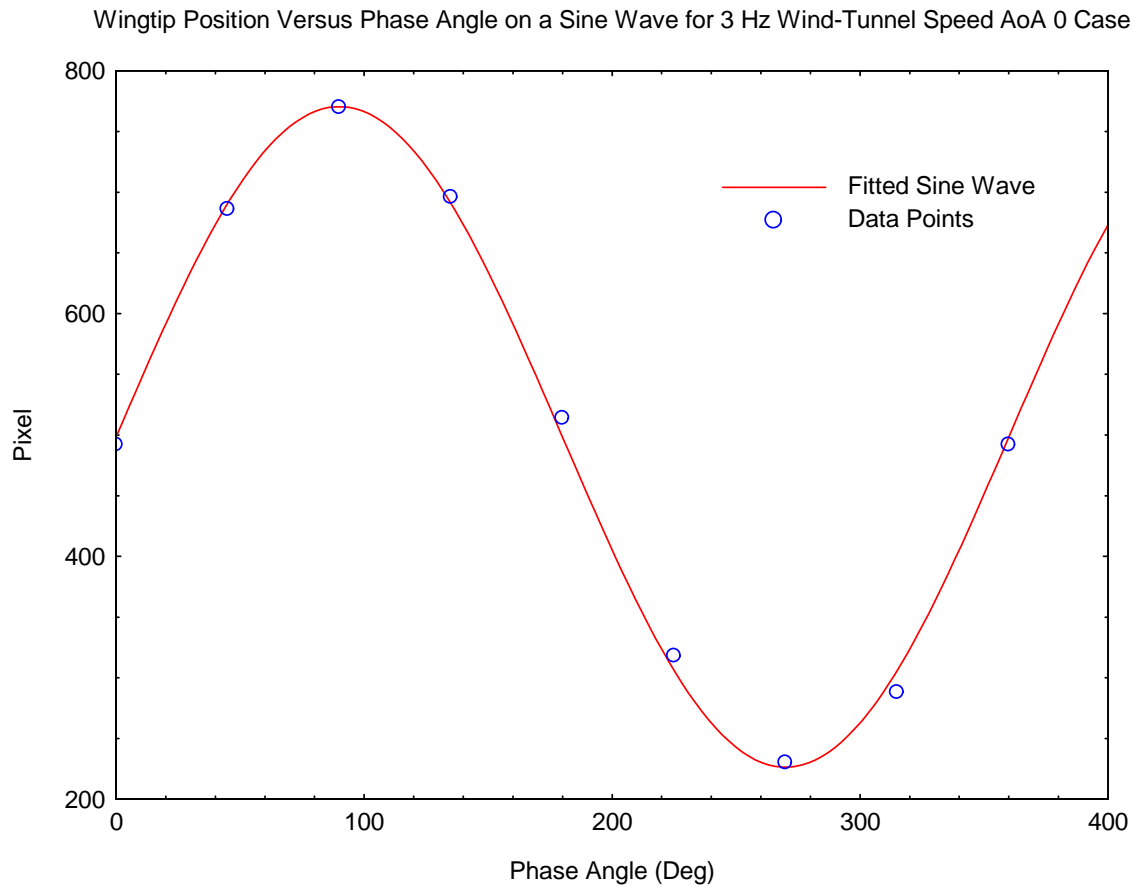
**Figure 6. Varying Wind-tunnel Velocity 3 Hz Motor Speed Case at AoA 0 Degrees
Wingtip Position Versus Phase Angle Plotted With Sine Curve**

Because of the limitations in the achievable wingtip velocities of the piezo fan the wind-tunnel was required to operate at lower speeds than it had previously been used at to achieve the flow conditions that would provide the desired advance ratios. At normal operation speeds for each Hz the wind-tunnel motor is operated at an equivalent number of m/s free-stream flow velocity is achieved. Because of the low speed conditions of the current study PIV was used to measure the free-stream velocity speed of the wind-tunnel at motor speeds between 0.5-5 Hz. It was found that at a motor speed of less than 0.6 Hz there is no flow in the wind-tunnel and by 5 Hz the speed was very close to 5m/s. A curve fit to the data

was used to allow for the calculation of any free-stream velocities desired to be selected by simple adjusting the wind-tunnel motor speed.
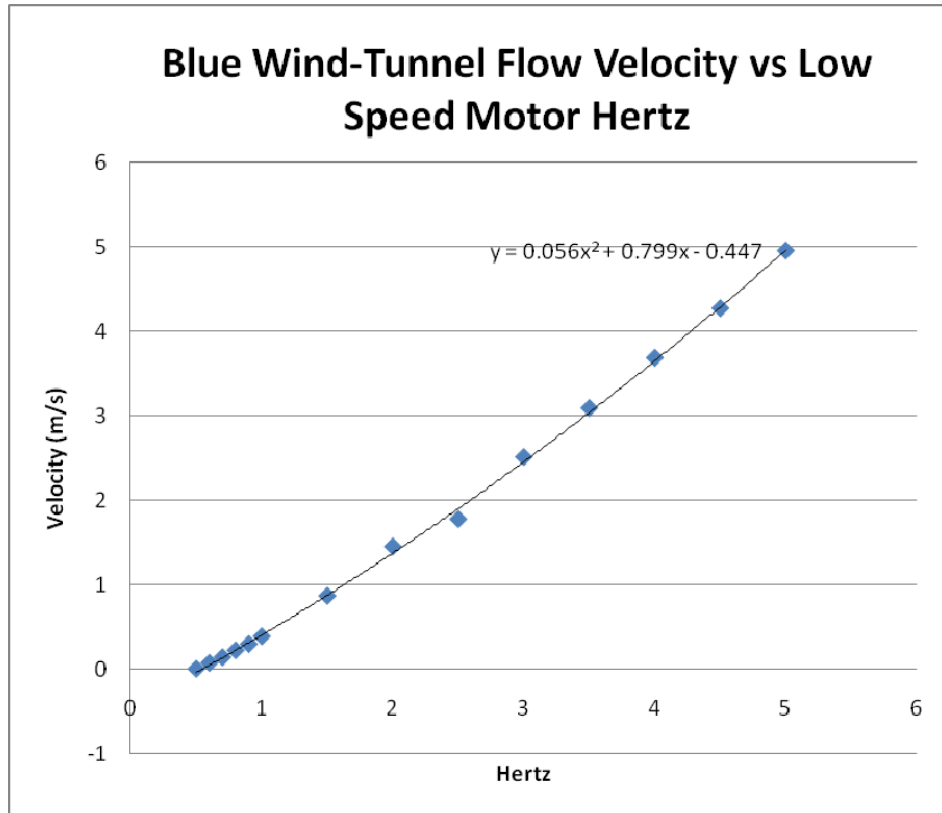
Figure 7. Wind-Tunnel Flow Velocity by Low Speed Motor Hz

To acquire the vortex structure of the flapping motion at different exact locations in the flapping motion the phase-angle was controlled by phase-locking the PIV system to the piezoelectric plate's motion. The phase-lock was achieved by driving both the piezoelectric plate and delay generator using a function generator. The piezoelectric plate will be at the same position in its movement, at a predetermined phase-angle, each time a PIV image pair is acquired. By adjusting the delay in the delay generator the position of the wingtip changes and the complete motion of the flapping can be captured. By taking a data set at a given

phase-angle the phased-averaged results show how the vortex sheet for a given experimental condition forms in what parts of the flapping motion.

The following illustration shows the experimental setup. For ease of use a second digital delay generator was used to select the phase by simply changing the delay between the function generator and main synchronizer.

Wind–Tunnel Test Section Walls

Flow direction is into image.

Laser Sheet

Piezo Fan

Camera

Power Amplifier

Optics

Laser

Mirror

Function Generator

Host Computer

Synchronizer

Delay Generator
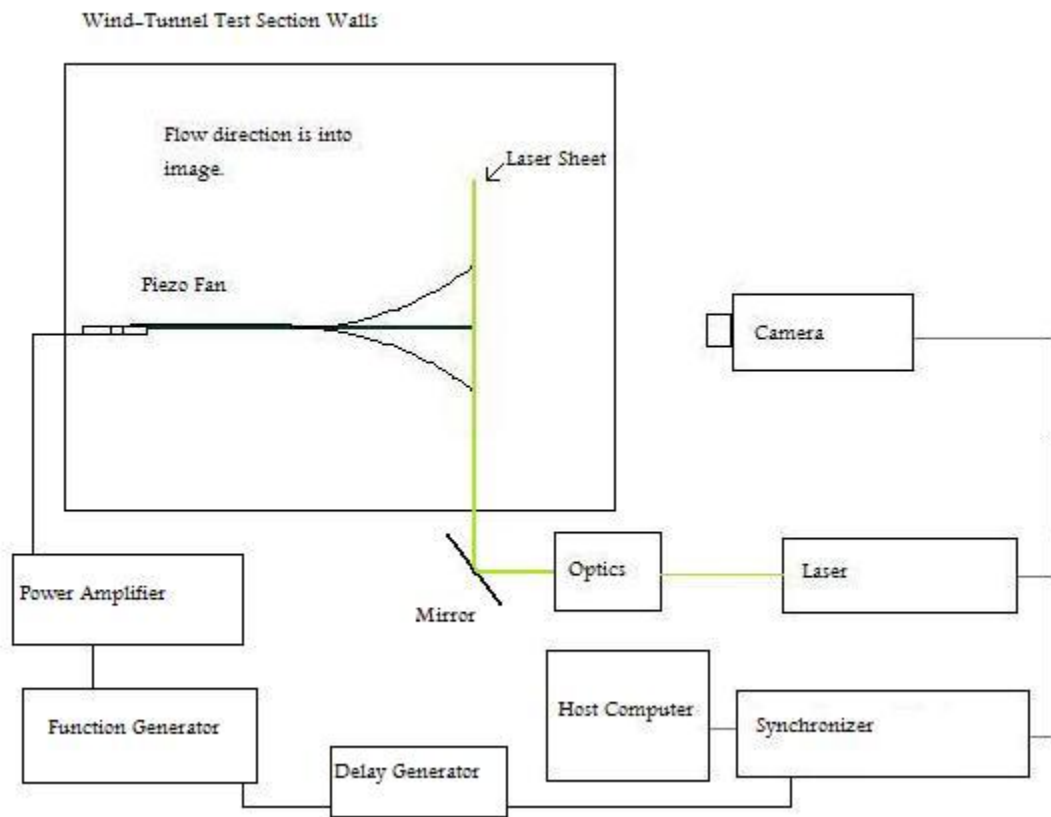
Figure 8. Illustration of the Experimental Setup

For clarity the mechanism the piezo fan was mounted on is not shown in the illustration but it is shown in the following figure. The rigid mount could be inserted into the side of the wind-tunnel test section and suspended the piezoelectric plate in the center of the test section. The design allowed for the AoA to be adjusted from outside of the test section

by rotating the entire circular center of the mount. The piezo fan and mount near the fan

were spray painted black to reduce laser reflection into the CCD camera.
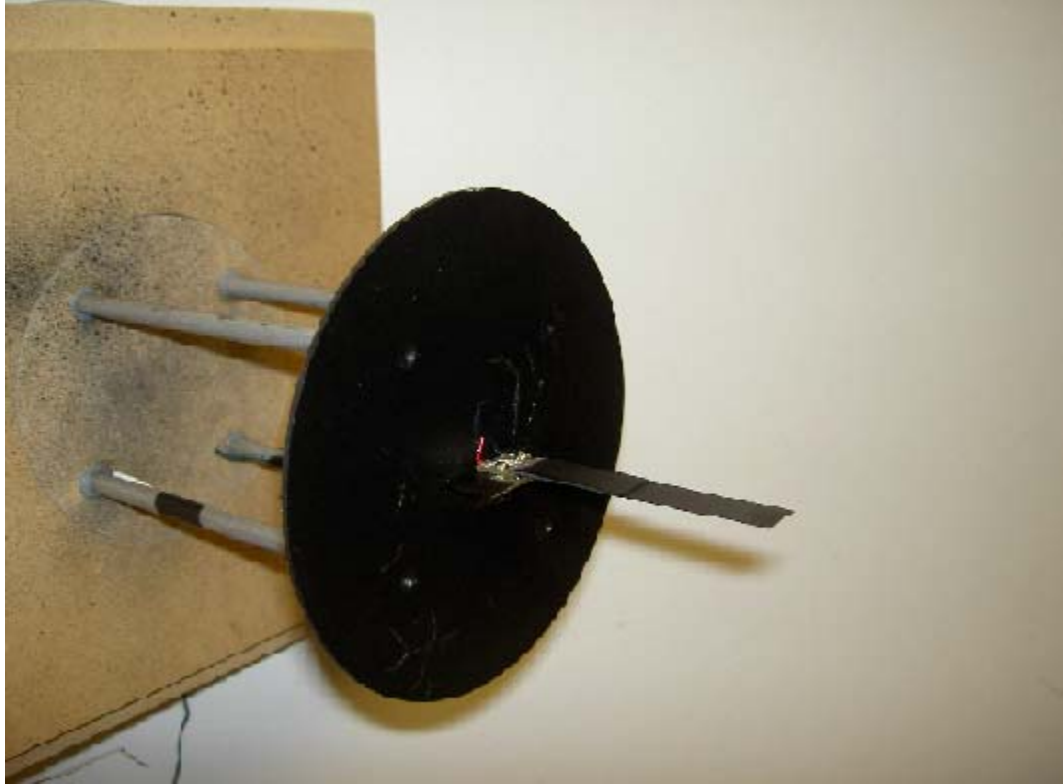
Figure 9. Mounted Piezo Fan

Experimental Design

In the first data set the experiment the conditions of J were changed by adjusting the

incoming speed in the wind-tunnel at 0, 10, and 20 degrees AoA. This data was used to

examine the effect of the change of V_∞ and AoA on the vortex wake structure. At each

condition of the following conditions phase-locked data for 8 phases was collected as well as

3 sets of instantaneous measurements were acquired for the purpose of calculating ensemble

averaged PIV results. Each data set taken for a given condition consisted of 166 PIV image

pairs.

Table 3. First Data Set Parameters at the Wingtip Location by V$_\infty$, AoA, f, A, Wingtip V, k, h, J, kh, Strouhal, and Re

Test	V$_\infty$ (m/s)	AoA (deg)	f (Hz)	A (m)	Wingtip V (m/s)	k	h	J	kh	Strouhal	Re
1	1.38	0	60	0.027	3.24	1.739	1.063	0.43	1.848	0.588	1156.4
2	2.46	0	60	0.027	3.24	0.974	1.063	0.76	1.035	0.329	2064.8
3	3.65	0	60	0.026	3.14	0.656	1.031	1.16	0.676	0.215	3068.1
4	4.96	0	60	0.022	2.66	0.483	0.871	1.87	0.421	0.134	4166.1
5	6	0	60	0.019	2.30	0.399	0.754	2.61	0.301	0.096	5040.9
6	8	0	60	0.014	1.74	0.299	0.570	4.60	0.171	0.054	6721.2
7	10	0	60	0.013	1.50	0.239	0.492	6.67	0.118	0.038	8401.5
8	1.38	10	60	0.027	3.24	1.739	1.063	0.43	1.848	0.588	1156.4
9	2.46	10	60	0.027	3.24	0.974	1.063	0.76	1.035	0.329	2064.8
10	3.65	10	60	0.026	3.14	0.656	1.031	1.16	0.676	0.215	3068.1
11	4.96	10	60	0.022	2.66	0.483	0.871	1.87	0.421	0.134	4166.1
12	6	10	60	0.019	2.30	0.399	0.754	2.61	0.301	0.096	5040.9
13	8	10	60	0.014	1.74	0.299	0.570	4.60	0.171	0.054	6721.2
14	10	10	60	0.013	1.50	0.239	0.492	6.67	0.118	0.038	8401.5
15	1.38	20	60	0.027	3.24	1.739	1.063	0.43	1.848	0.588	1156.4
16	2.46	20	60	0.027	3.24	0.974	1.063	0.76	1.035	0.329	2064.8
17	3.65	20	60	0.026	3.14	0.656	1.031	1.16	0.676	0.215	3068.1
18	4.96	20	60	0.022	2.66	0.483	0.871	1.87	0.421	0.134	4166.1
19	6	20	60	0.019	2.30	0.399	0.754	2.61	0.301	0.096	5040.9
20	8	20	60	0.014	1.74	0.299	0.570	4.60	0.171	0.054	6721.2
21	10	20	60	0.013	1.50	0.239	0.492	6.67	0.118	0.038	8401.5

To measure the effects of span-wise location a second data was taken as in the above

data set, by adjusting the wind-tunnel free-stream velocity and the AoA to achieve the

desired conditions. The laser sheet was adjusted to illuminate the three-quarter and half

span-wise locations on the piezoelectric plate thereby not requiring any changes inside the

wind-tunnel to the specimen or mount to achieve these measurements. The span-wise test

conditions are shown in Table 4 and Table 5 below. It is important to note that the function

generator was not available at the time this data set was taken and instantaneous results are

used to analyze the vortex structure as phase-angle controlled measurements were not

possible.

Table 4. Three-quarter Span-wise Location Data Parameters by V_∞, AoA, f, A, k, h, J, kh, Strouhal, and Re

Test	V_∞ (m/s)	AoA (deg)	f (Hz)	A (m)	k	h	J	kh	Strouhal	Re
				0.75 Span-wise Location						
1	0.53	0	60	0.008	4.535	0.327	0.53	1.482	0.472	443.5
2	1.05	0	60	0.008	2.271	0.327	1.06	0.742	0.236	885.7
3	2.64	0	60	0.008	0.906	0.327	2.65	0.296	0.094	2219.0
4	5.28	0	60	0.008	0.454	0.327	5.30	0.148	0.047	4394.0
5	0.53	10	60	0.008	4.535	0.327	0.53	1.482	0.472	443.5
6	1.05	10	60	0.008	2.271	0.327	1.06	0.742	0.236	885.7
7	2.64	10	60	0.008	0.906	0.327	2.65	0.296	0.094	2219.0
8	5.28	10	60	0.008	0.454	0.327	5.30	0.148	0.047	4394.0
9	0.53	20	60	0.008	4.535	0.327	0.53	1.482	0.472	443.5
10	1.05	20	60	0.008	2.271	0.327	1.06	0.742	0.236	885.7
11	2.64	20	60	0.008	0.906	0.327	2.65	0.296	0.094	2219.0
12	5.28	20	60	0.008	0.454	0.327	5.30	0.148	0.047	4394.0

Table 5. Half Span-wise Location Data Parameters by V_∞, AoA, f, A, k, h, J, kh, Strouhal, and Re

Test	V_∞ (m/s)	AoA (deg)	f (Hz)	A (m)	k	h	J	kh	Strouhal	Re
				0.5 Span-wise Location						
1	0.53	0	60	0.006	4.535	0.217	0.80	0.982	0.313	443.5
2	1.05	0	60	0.006	2.271	0.217	1.60	0.492	0.157	885.7
3	2.64	0	60	0.006	0.906	0.217	4.00	0.196	0.062	2219.0
4	5.28	0	60	0.006	0.454	0.217	7.99	0.098	0.031	4394.0
5	0.53	10	60	0.006	4.535	0.217	0.80	0.982	0.313	443.5
6	1.05	10	60	0.006	2.271	0.217	1.60	0.492	0.157	885.7
7	2.64	10	60	0.006	0.906	0.217	4.00	0.196	0.062	2219.0
8	5.28	10	60	0.006	0.454	0.217	7.99	0.098	0.031	4394.0
9	0.53	20	60	0.006	4.535	0.217	0.80	0.982	0.313	443.5
10	1.05	20	60	0.006	2.271	0.217	1.60	0.492	0.157	885.7
11	2.64	20	60	0.006	0.906	0.217	4.00	0.196	0.062	2219.0
12	5.28	20	60	0.006	0.454	0.217	7.99	0.098	0.031	4394.0

To study the effect of amplitude on the vortex structure a third data set was taken

where the wind-tunnel velocity was maintained at 2.46 m/s and the voltage fed to the

piezoelectric plate from the function generator was varied. By decreasing the voltage the

amplitude of the flapping motion also decreased. These measurements were taken at the

wingtip of the piezoelectric plate and the AoA was kept at 0 degrees. The experimental

conditions for the varying amplitude data set are found below in Table 6.

Table 6. PIV Data for Varying Amplitude by V$_\infty$, AoA, f, A, Wingtip V, k, h, J, kh, Strouhal, and Re

Test	V$_\infty$ (m/s)	AoA (deg)	f(Hz)	A(m)	Wingtip V (m/s)	k	h	J	kh	Strouhal	Re
1	2.46	0	60	0.024	2.88	0.973	0.945	0.87	0.905	0.288	2064.8
2	2.46	0	60	0.019	2.23	0.973	0.73	1.12	0.699	0.223	2064.8
3	2.46	0	60	0.013	1.54	0.973	0.504	1.63	0.483	0.154	2064.8
4	2.46	0	60	0.008	0.92	0.973	0.301	2.73	0.288	0.092	2064.8
5	2.46	0	60	0.002	0.30	0.973	0.098	8.4	0.094	0.030	2064.8

Figure 10 shows the voltage fed to the piezoelectric plate verses the flapping

amplitude observed. This is a linear relationship as expected for a piezoelectric material a

voltage causes a proportional mechanical stress. This plots the five data points for the

voltages of 180, 140, 100, 60, and 20 volt in the reduced amplitude data set plus the full 200

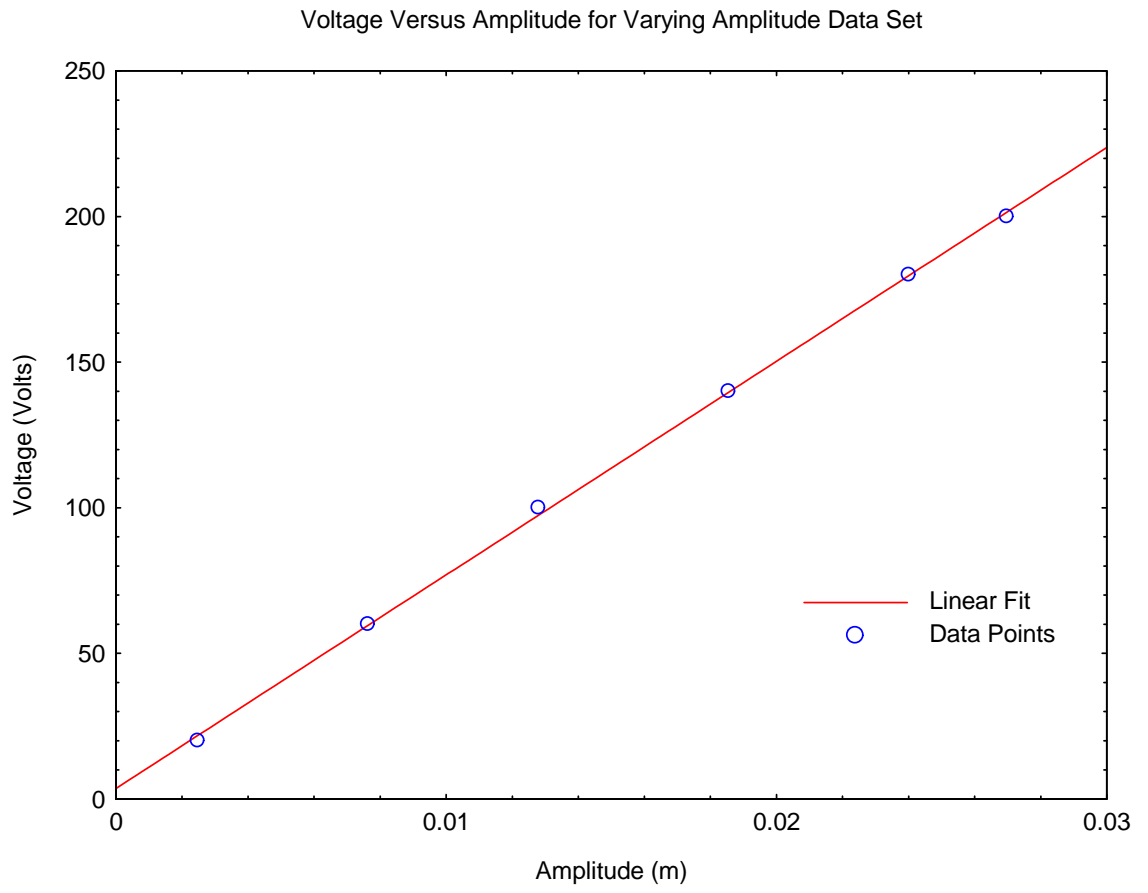volt amplitude at the same wind-tunnel conditions of 3 Hz motor speed.

Figure 10. Voltage Versus Amplitude for Varying Amplitude Data Set With Linear Fit

CHAPTER 4. RESULTS

The experimental results of the current study are presented here. The results are further discussed in the Conclusions section of chapter five.

Amplitude Effect

The advance ratio for a given flapping plate condition will change with changing amplitude as the flapping amplitude and frequency determine the speed of the flapping motion of the plate. When thinking of the amplitude effect on wake structures of a flapping plate how do the results of the present study compare to previous works? How do the resulting wake structures from varying the amplitude to change J differ from those from varying the incoming flow velocity to change J? What effect do different sized amplitudes have on the vortex wake structure? To answer these questions the following experimental results were gathered.

The study of the amplitude effect was done at zero AoA. With constant wind-tunnel velocity of 2.5 m/s the change in advance ratio for this study depends only on the controlled changing flapping amplitude. Decreasing the flapping amplitude reduces the wingtip speed of the piezoelectric plate and thus increases J. This was accomplished by reducing the voltage given by the function generator, reducing the amplitude of the sin wave function and thus reducing the flapping amplitude of the piezoelectric plate. As the advance ratio increases it has been shown by Lai and Platzer (1999) that the result of the changing vortex wake structure is to go from thrust, to neutral, to drag generating vortex sheets. The mean velocities shown in Figure 11 show that as advance ratio decreases with increasing A that the

two jet-like plumes released from the wake of the plate increase in magnitude. The mean

velocity for the largest J of 8.40 shows no jet like plumes at all only a decreased velocity

magnitude wake directly downstream from the plate which is indicative of a drag wake.

Comparing these indicated drag wakes from the mean velocity data for high advance ratios

from this amplitude effect study to those from the V_∞ effect found in Figure 19 shows that at

J of 4.6 and 6.67 have the same lack of the two diverging jets found at the lower advance

ratios and instead have a similar velocity field to that from the J=8.40 case found here. The

relative intensity of the jet structures increases with decreasing J in both studies. The mean

velocity magnitude data implies more thrust is generated at lower J which is also shown to be

the case in the mean-velocity profiles found in Figure 14. The profiles were taken two chord

lengths downstream from the trailing edge of the piezoelectric plate. The turbulent kinetic

energy shown in Figure 12 increases with decreasing J and the angle that the jet plumes

diverge at can also be seen to increase with decreasing J. There is very little turbulence in

the drag like wake of J=8.40 while the thrust jets found in the lower advance ratios are

inherently turbulent. At any of the J tested the highest levels of turbulence are concentrated

at or just behind the trailing edge of the piezoelectric flapping plate. The change in the

plume angle is caused in this case by the shrinking size of the vortex structure with smaller

flapping amplitudes as can be seen in the phase-angle vorticity plots. The phase-angles

showing the vortex structures for three select cases are found in Figure 13. The selected

cases were chosen as to show different types of vortex structure and to not repeat similar

cases. At a J of 8.40 the wake structure is clearly seen to be a von Kármán vortex sheet with

negative vortices over positive shown at all four phases. The wake structure is comparatively

small to the PIV image size at this low amplitude and the drag wake is confirmed in Figure

14 as there is a large velocity deficit about y/c=1 in height. Between the select cases in

Figure 13 and the velocity profiles found in Figure 14 the case is made that as the amplitude

increases and J decreases the wake structure grows in size. For J of 2.73 as seen in Figure 12

the two small jets above and below the velocity deficient (drag) between them together make

the wake structure over y/c=2.5 in height as shown in the velocity profile in Figure 14. The

vortex structure for J=2.73 seen in Figure 13 appears to be forming into a nearly neutral wake

structure as there are two rows forming with alternating sign vortices whose vortex pairs are

oriented nearly parallel to the flow direction. The negative vortices form on the upper

surface of the piezoelectric plate and the positive on the lower surface. At 90 deg phase

angle both a positive and negative vortices is shed with the positive slightly behind and

below the negative. As the plate flaps downward the vortices shed at 90 deg phase angle

move upward slightly from the position they were shed and the positive vortex moves into

position behind the negative. At 270 degree phase angle (bottom of the flapping motion) the

opposite occurs where both a positive from the lower surface and a negative from the upper

surface vortices are shed but this time the positive is first with the negative just behind and

above it. As the plate continues flapping upper this vortex pair moves slightly downward

from where it was shed as the negative vortex moves into position behind the positive. The

resulting structure is identified as a drag inducing wake structure by both the definition of a

neutral wake structure where two vortices of the same sign (whereas in this case opposite

sign shedding is seen) should be shed at top and bottom and by the slightly negative result of

the velocity profile. This wake structure is nearly an identical match for that seen in Lai and

Platzer (1999) figure 3a whose experimental conditions are compared in the Table 7 below.

Because of the discrepancies in h, k, and Re it is impossible to say what effect the amplitude

played in this but it is clear that there is an important effect of another experimental condition

other than the advance ratio for these two very different cases to have nearly identical vortex

wake structures. At the J in value in this case by Lai and Platzer (1999) the present study has

a vortex structure as seen in the J=8.40 case of a merged von Kármán vortex sheet.

Table 7. Data Set Conditions Comparison Between Wake Structure Case of Lai and Platzer (1997) and Present Study

	A (m)	h	k	kh	Strouhal	J	Re
Lai and Platzer	0.003	0.0125	7.84	0.098	0.031	8.01	20000
Clemons	0.008	0.3008	0.973	0.288	0.0917	2.73	2064.8

At J=0.77 the wake structure is much larger than the PIV image window. Only part

of the wake profile in Figure 14 is captured on the image but from what is available there is a

velocity surplus. Because behind the trailing edge only x/A<2 worth of data has been

captured the vortex structure does not develop into a recognizable structure though because

of the wake profile a reverse von Kármán vortex sheet would be expected to develop as this

is a thrust generating vortex sheet. However, analysis of the vortex shedding in Figure 13

shows many similarities from the J=2.73 case. While still two vortices of opposite sign are

shed at the top and bottom the differences can be seen in the positive vortex shed at the top

and the negative vortex shed at the bottom are still attached to the plate when it has returned

to the center position 90 deg later. Also at a phase angle of 180 and 270 the negative vortex

forming on the upper surface can be seen to detach and reattach to the plate forming a

separation bubble. Otherwise it appears that the vortices are much stronger in this case and

begin noticeably forming at the leading edge rather than mid-chord of the plate. The only

case in Lua ET AL(2007) to have similar conditions of h and J to those found in the present

study match well to this case, h=1.1 and J=0.91 in their case to the present case of J=0.77 and

h=1.06. Lua ET AL (2007) identified this condition as a reverse von Kármán vortex sheet structure. Looking at the vortex shedding for the case from Lua ET AL (2007) there is good agreement between their results and the results of the present study. A comparison of the conditions found in these two cases is shown below in Table 8 below.

Table 8. Comparison of Experimental Conditions for Cases Between Lua ET AL and the Present Study

	A (m)	h	kh	Strouhal	J	Re
Lua ET AL	0.044	1.104	0.867	0.276	0.91	1000
Clemons	0.027	1.063	1.035	0.329	0.76	2064.8

The results of the present study both compare well with the previous works of others on heaving airfoils and show the importance of the effect of amplitude (as well as frequency) on the vortex structure by showing how very different conditions of J, h, and k can lead to similar results. The comparison of the amplitude effect and V_∞ effect will be discussed in the V_∞ effect section. The effect of the amplitude on the results of the vortex structure in the wake of a piezoelectric plate is that decreasing amplitude results in increasing J values, given all else is constant, and leads to smaller vortices and vortex wake structures.

a). A=2.48mm J=8.40

b). A=7.64mm J=2.78

c). A=12.80mm J=1.68

d). A=18.66mm J=1.12

e). A=24.01mm J=0.87

f). A=26.99mm J=0.77
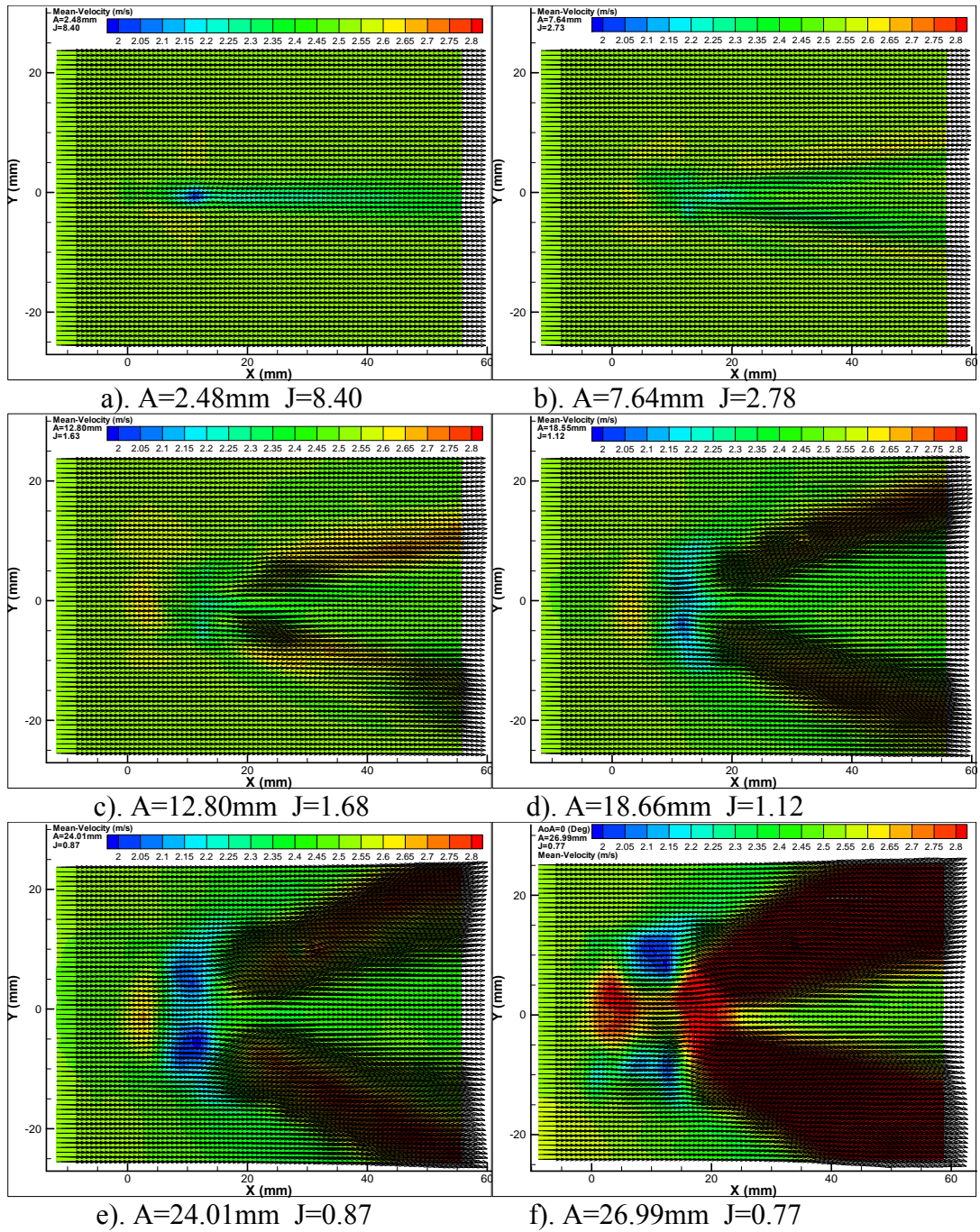
Figure 11. Mean-Velocity Magnitudes of Varying Amplitude Data Sets

a). A=2.48mm J=8.40

b). A=7.64mm J=2.78

c). A=12.80mm J=1.68

d). A=18.66mm J=1.12

e). A=24.01mm J=0.87

f). A=26.99mm J=0.77
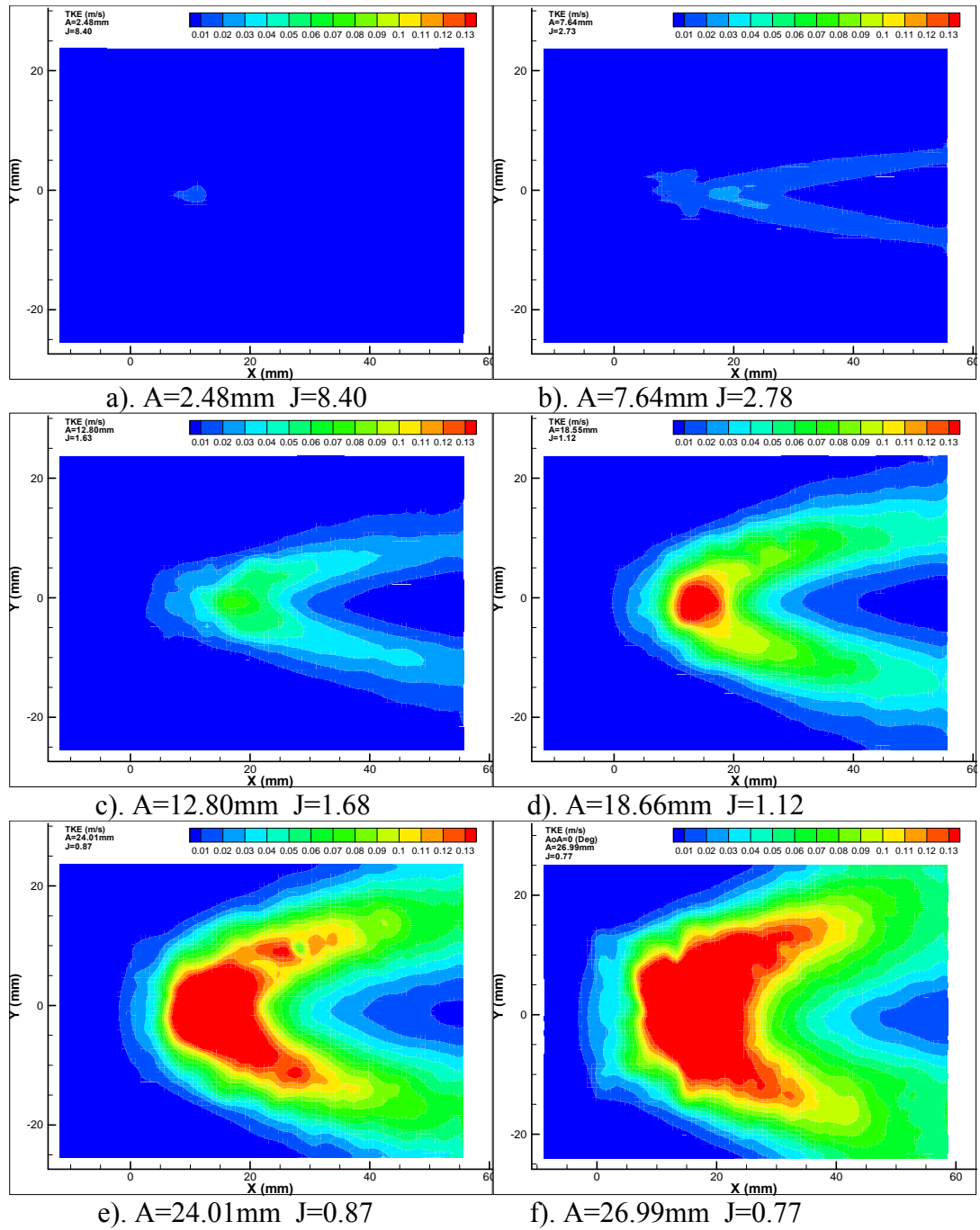
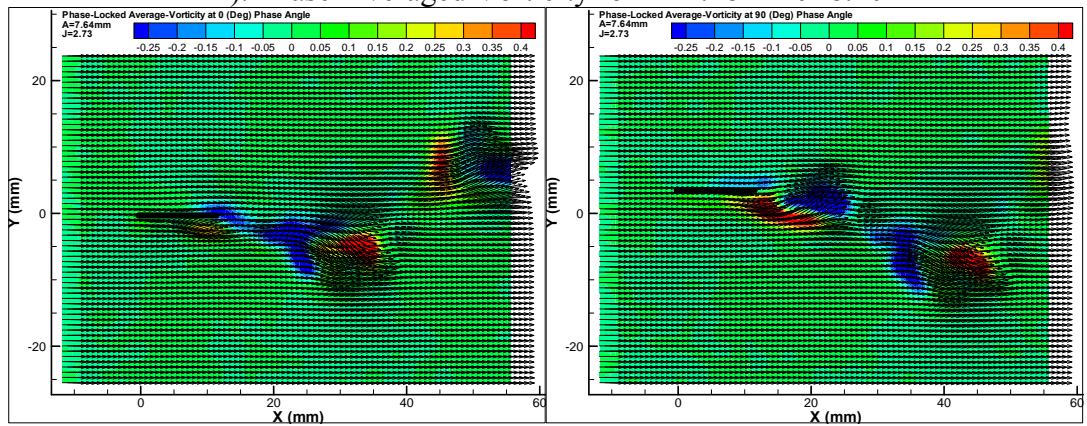**Figure 12. Turbulent Kinetic Energy of Varying Amplitude Data Set**
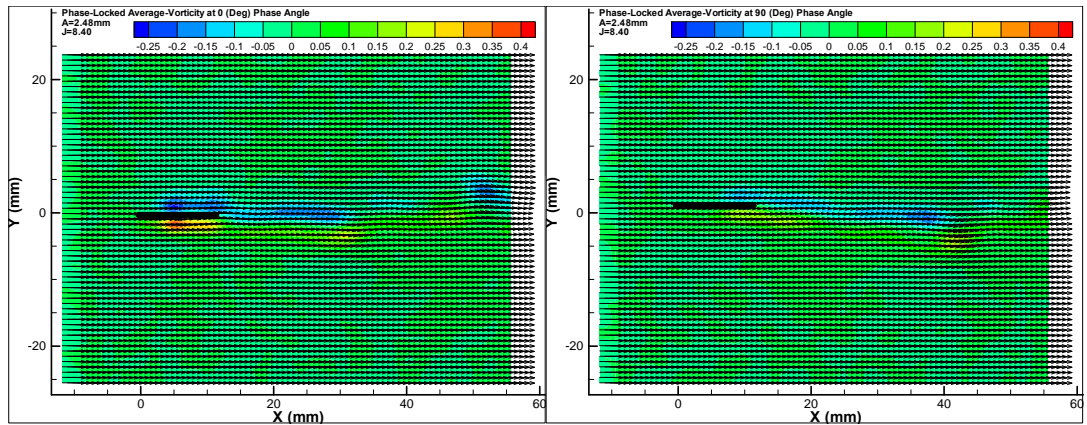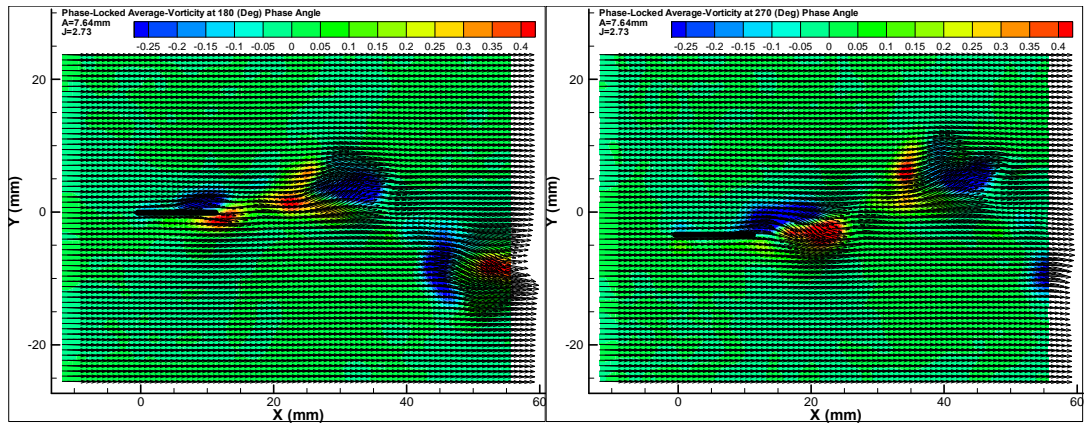
a). 0 Degree Phase Angle   b). 90 Degree Phase Angle
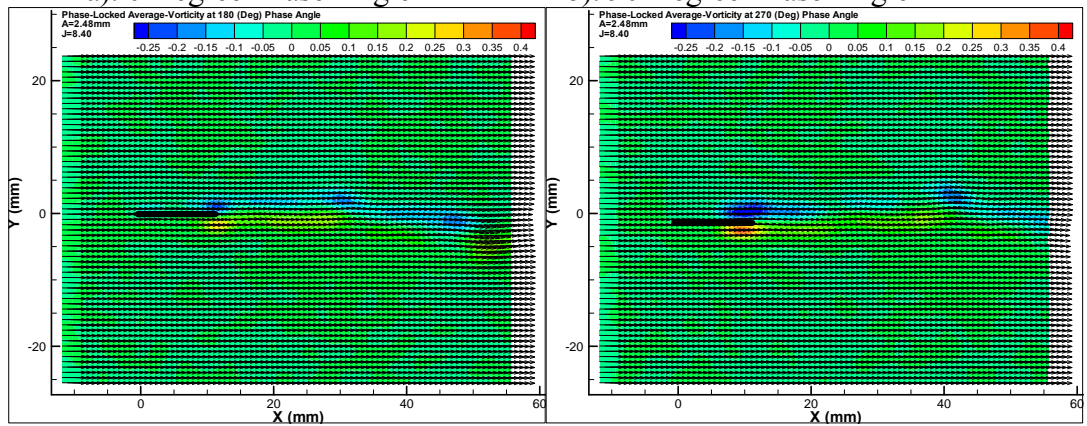
c). 180 Degree Phase Angle   d). 270 Degree Phase Angle

A). Phase-Averaged Vorticity for A=2.48mm J=8.40

a). 0 Degree Phase Angle   b). 90 Degree Phase Angle

c). 180 Degree Phase Angle　　　　d). 270 Degree Phase Angle

B). Phase-Averaged Vorticity for A=7.64mm J=2.73
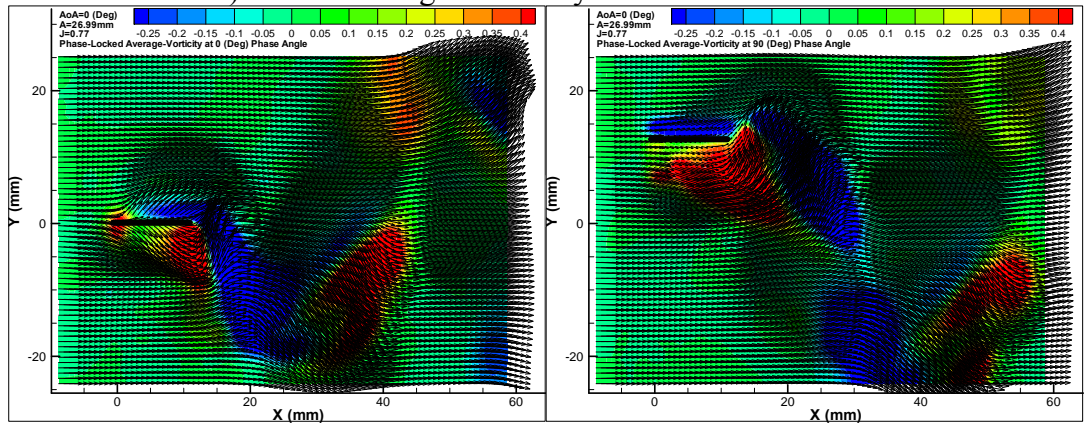
a). 0 Degree Phase Angle　　　　b). 90 Degree Phase Angle
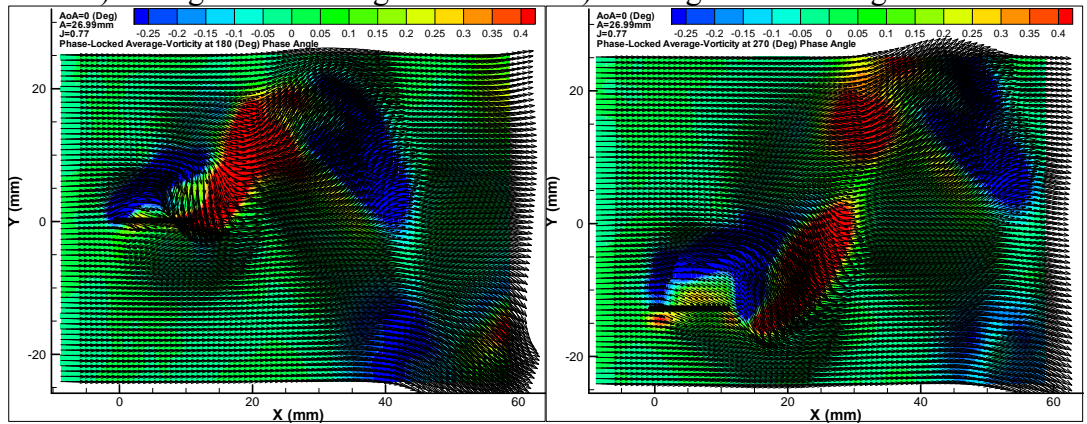
c). 180 Degree Phase Angle　　　　d). 270 Degree Phase Angle

C). Phase-Averaged Vorticity for A=26.99mm J=0.77

Figure 13. Phased-Averaged Vorticity at 0, 90, 180, and 270 degree Phase Angles for Select Varying Amplitude Cases

Mean Veolcity Profiles for Varying Amplitude Data Set
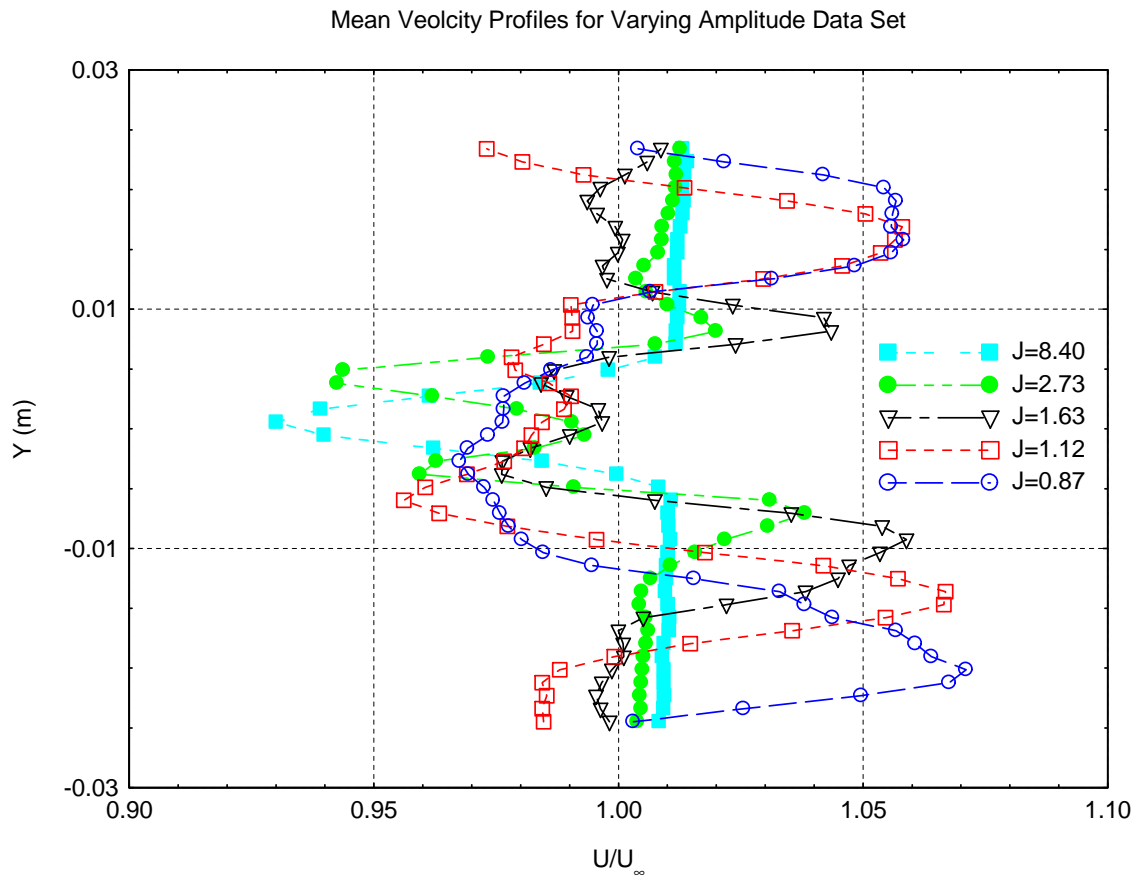
Figure 14. Mean Velocity Profiles for Varying Amplitude Cases

Span-wise Effect

Of note is that this data set does not include phase-averaged data and instead uses an ensemble-average of five-hundred PIV images to measure the average velocity profiles. When looking at the effects of the span-wise location how do the results compare by location for the same conditions of flapping and wind-tunnel velocity? Are their changes in the vortex structure by span-wise location and if so are these simply due to the decreased flapping amplitude found as your move further away from the wingtip? How do these results compare to the literature and other experimental conditions with similar advance ratios from the present study?

In Figure 15 to Figure 18 the results showing dependence on span-wise location to the vortex wake structure of the piezoelectric flapping plate are shown. The smaller flapping amplitudes found at the half or three-quarter span cause the structure to develop more rapidly downstream as x/A decreases, allowing for better identification of the vortex structures given the limitations in the PIV window viewing wake structures at higher flapping amplitudes as these develop too far downstream from the trailing edge of the piezoelectric flapping plate. It can be seen in Figure 15 the wake structure varies based on span-wise location for the same conditions of amplitude and wind-tunnel velocity. The wake structures identified here are from instantaneous vorticity results as the phase-averaged results are not available for the span-wise effect data set. At the wingtip there is a complex shedding of multiple vortices that results in a jet like thrust producing wake structure. At the half span location the wake structure rapidly dissipates within x/c=1.5 and it has very little jet like properties as seen in the ensemble-averaged velocity profile. The wake structure at the three quarter span-wise

location is a combination of both structures. There are both a strong dipole whose vortices annihilate one another, dissipating rapidly, as well as multiple smaller vortexes shed that do not dissipate as rapidly. In Figure 16 at a higher wind-tunnel velocity giving advance ratios around one, a reverse von Kármán can be identified by the two rows of alternating vortices with the anti-clockwise (positive) above and the clockwise (negative) below. At the half span these signs change farther downstream and as can be seen in the ensemble averaged data a von Kármán. These structures can be seen very clearly at the half location and as the image plane moves out to the three-quarter span locations it becomes more convoluted by multiple vortexes shed per cycle, especially when the measurement location moves out to the wingtip. These two cases strongly point to dependence on span-wise location of the flow phenomenon as such results were not found in the decreased amplitude cases at the wingtip. In Figure 17 the vortex structures at advance ratios between 2 and 4 are a complex multiple vortices shed per half cycle neutral wake. The wake structures found at J=4 are all von Kármán vortex sheets. At J=2 and J=4 there seems to not be a dependence on span-wise location of the vortex wake structure type but the intensity of the jet like structure increases for all four advance ratios as the image plane approaches the wingtip. In Figure 18 the average-velocity profiles are given for the first two cases. The area under the curve that is greater than one increases as the measurement location moves toward the wingtip indicating that the larger amplitude there does generate more thrust than at other locations on the piezoelectric airfoil.

Not only does the vortex structure type vary span-wise for the same condition which may point to a dependence on amplitude to the vortex structure, but also the vortex structure seen at similar amplitudes and advance ratios between cases from this and the varying

amplitude data set have different results. For example, at the wingtip location from the

varying amplitude data set the J=2.73 and h=0.301 the vortex structure is very clearly a drag

wake seen in Figure 13 while at the three-quarter span-wise location seen in Figure 17 the

mean-velocities show a small jet of greater velocity magnitude in the wake for the very

similar conditions of J=2.65 and h=0.327. A third case, from Lua ET AL (2007), those it has

about half the h it has a very similar advance ratio and the researchers identified a thrust

generating reverse von Kármán vortex sheet in that case. Because the heaving airfoil cases

of previous studies are two dimensional as opposed to the three dimensional flapping motion

found in the current study there is no direct comparison of span-wise location effect results

from those studies. In Table 9 the three similar cases experimental conditions are presented

for purpose of comparison.

Table 9. Experimental Data Set Conditions for Three Similar Cases by A, k, h, J, kh, Strouhal, and Re

	A (m)	k	h	J	kh	Strouhal	Re
0.75 Span-wise Location	0.008	0.906	0.327	2.65	0.296	0.094	2219.0
Wingtip	0.008	0.973	0.301	2.73	0.288	0.092	2064.8
Lua ET AL	0.007	1.571	0.184	2.72	0.289	0.092	1000

With nearly identical k, h, and J the vortex wake structure between the varying

amplitude case at the wingtip and the 0.75 span-wise location should be similar as was shown

between similar cases from this and previous studies in the amplitude effect discussion.

However the results from the conditions in Table 9 show the 0.75 span-wise case to have

similar vortex structure properties to the Lua ET AL (2007) case with h value nearly half the

size.   The cause of this phenomenon is unclear and merits further study.

The vortex wake structure was found to vary down the span of the piezoelectric plate for the same wind-tunnel velocity although the structures found here were not directly comparable to the varying amplitude results suggesting that the change in amplitude is not solely responsible for the change in wake structures. More research is needed to be able to understand the span-wise location effect on the wake structures of the piezoelectric plate to make meaningful comparisons with other results.
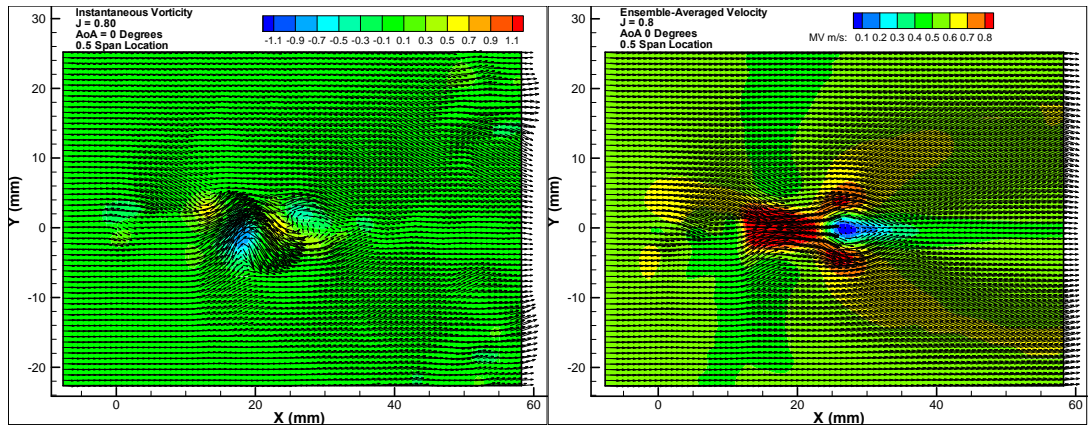
a). Instantaneous flow field   b). Ensemble-averaged flow field

A: Streamwise plane at 0.50 of the wing span
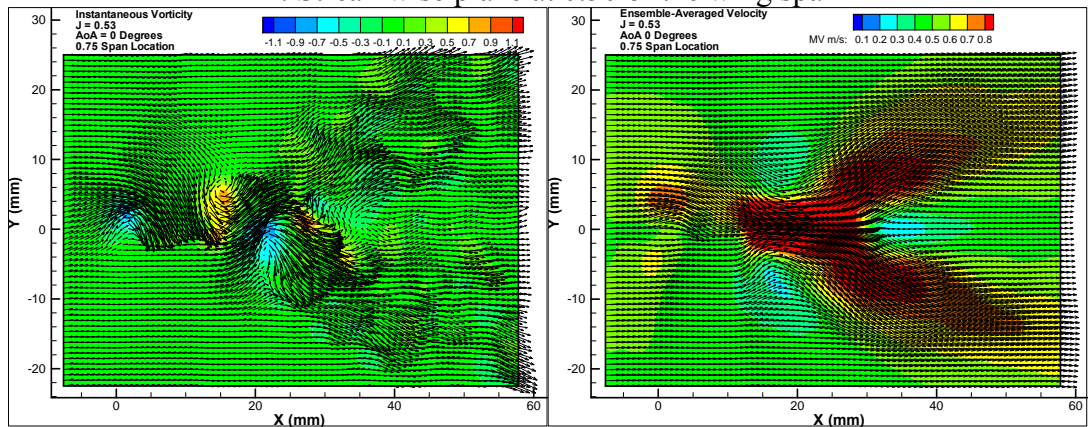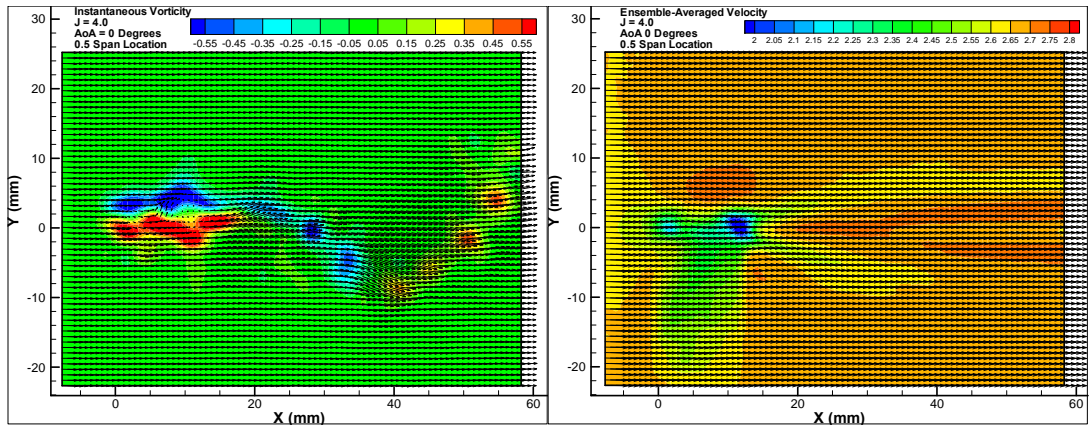
a). Instantaneous flow field   b). Ensemble-averaged flow field

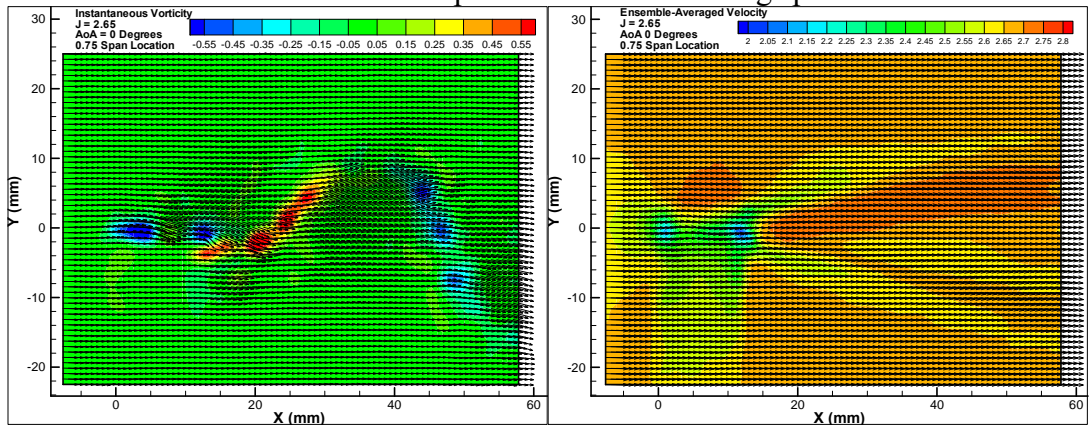B: Streamwise plane at 0.75 of the wing span
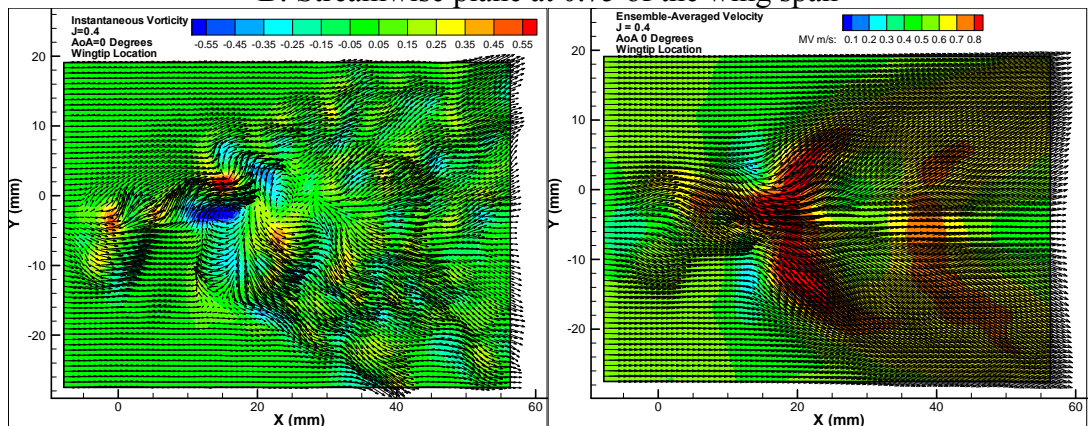
a). Instantaneous flow field   b). Ensemble-averaged flow field
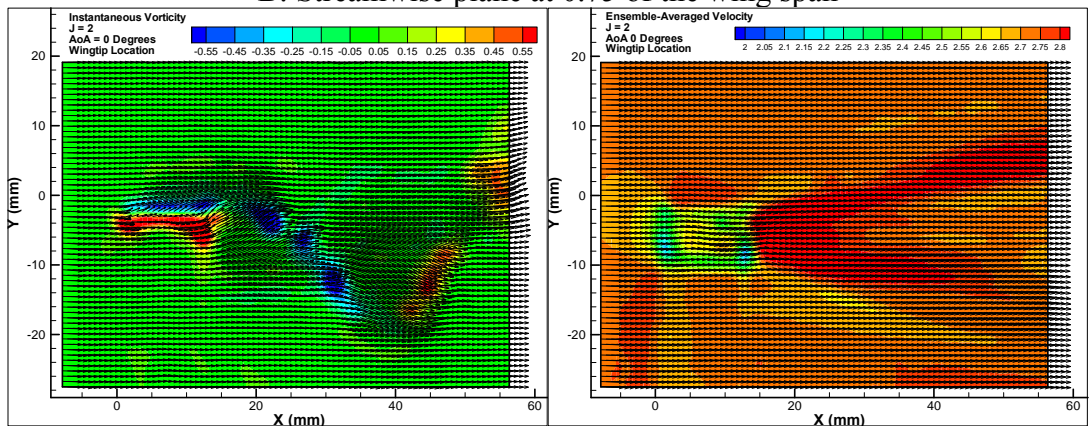
C: Streamwise plane at 1.0 of the wing span (wingtip)

Figure 15. Instantaneous Vorticity and Ensemble-Averaged Velocity at V_∞=0.53m/s and AoA of 0 Degrees by Span-wise Location
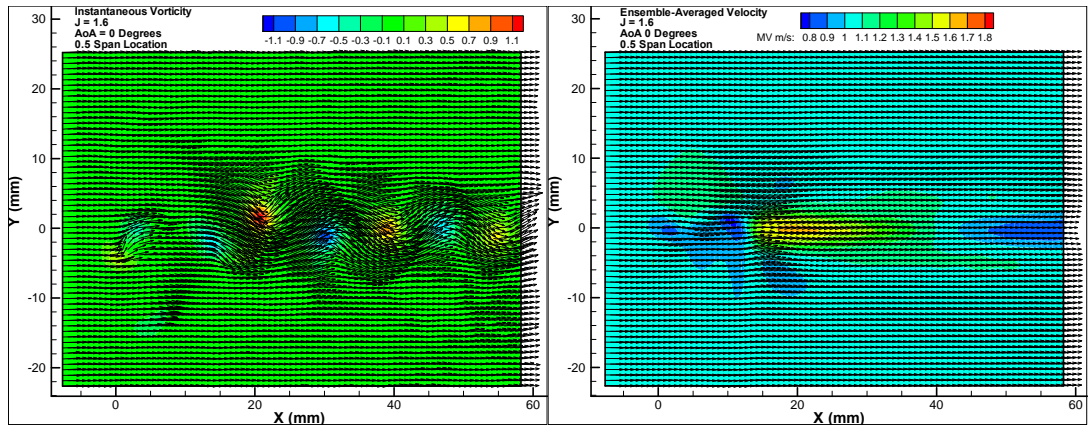
a). Instantaneous flow field   b). Ensemble-averaged flow field

A: Streamwise plane at 0.50 of the wing span
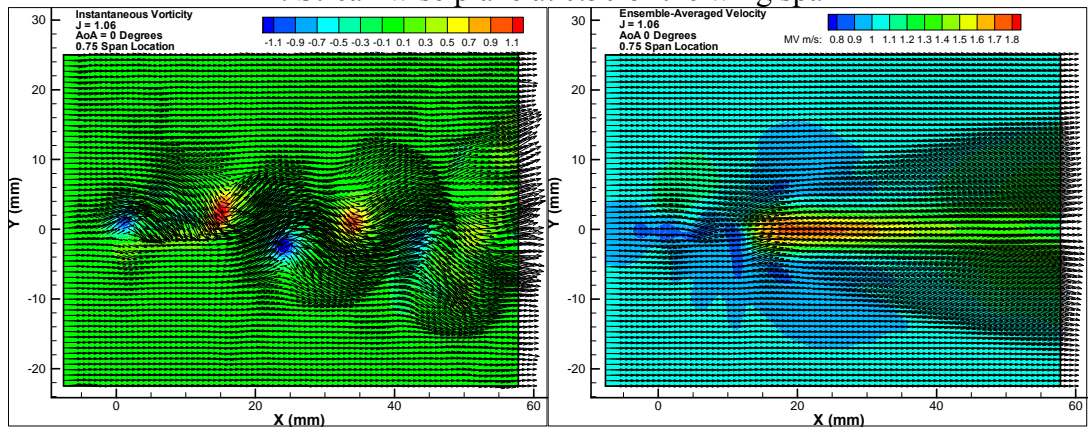
a). Instantaneous flow field   b). Ensemble-averaged flow field

B: Streamwise plane at 0.75 of the wing span
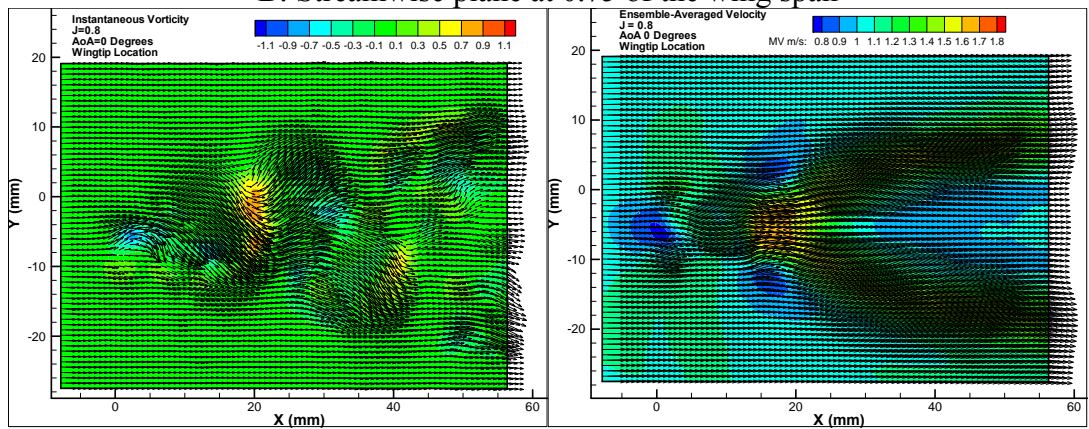
a). Instantaneous flow field   b). Ensemble-averaged flow field

C: Streamwise plane at 1.0 of the wing span (wingtip)

Figure 16. Instantaneous Vorticity and Ensemble-Averaged Velocity at V_∞=1.05m/s and AoA of 0 Degrees by Span-wise Location

a). Instantaneous flow field   b). Ensemble-averaged flow field

A: Streamwise plane at 0.50 of the wing span

a). Instantaneous flow field   b). Ensemble-averaged flow field

B: Streamwise plane at 0.75 of the wing span

a). Instantaneous flow field   b). Ensemble-averaged flow field

C: Streamwise plane at 1.0 of the wing span (wingtip)

Figure 17. Instantaneous Vorticity and Ensemble-Averaged Velocity at V_∞=2.64m/s and AoA of 0 Degrees by Span-wise Location
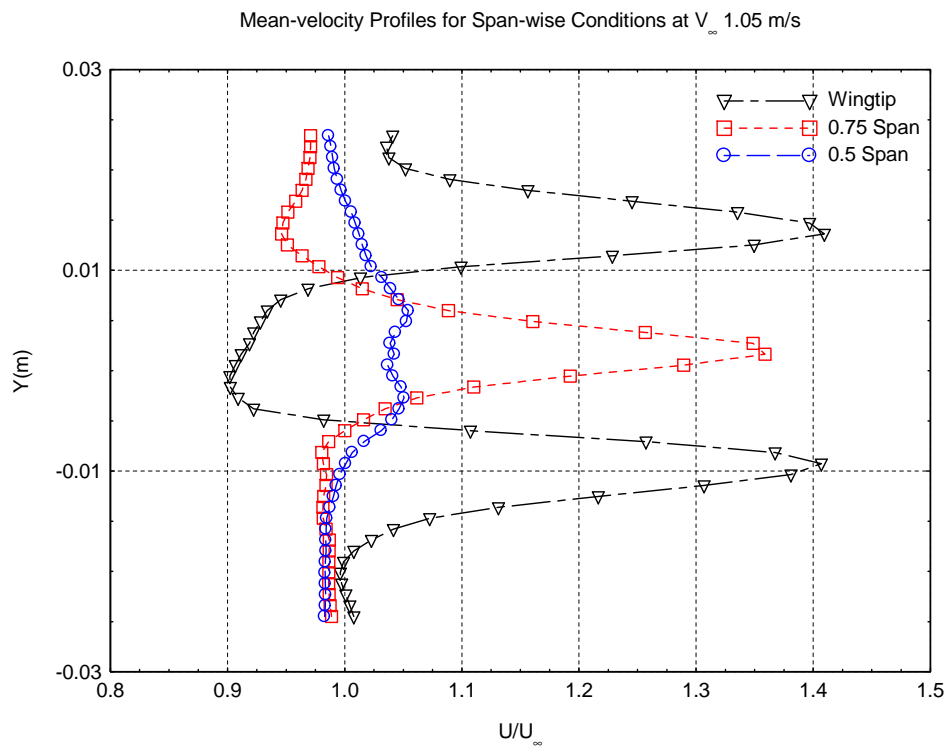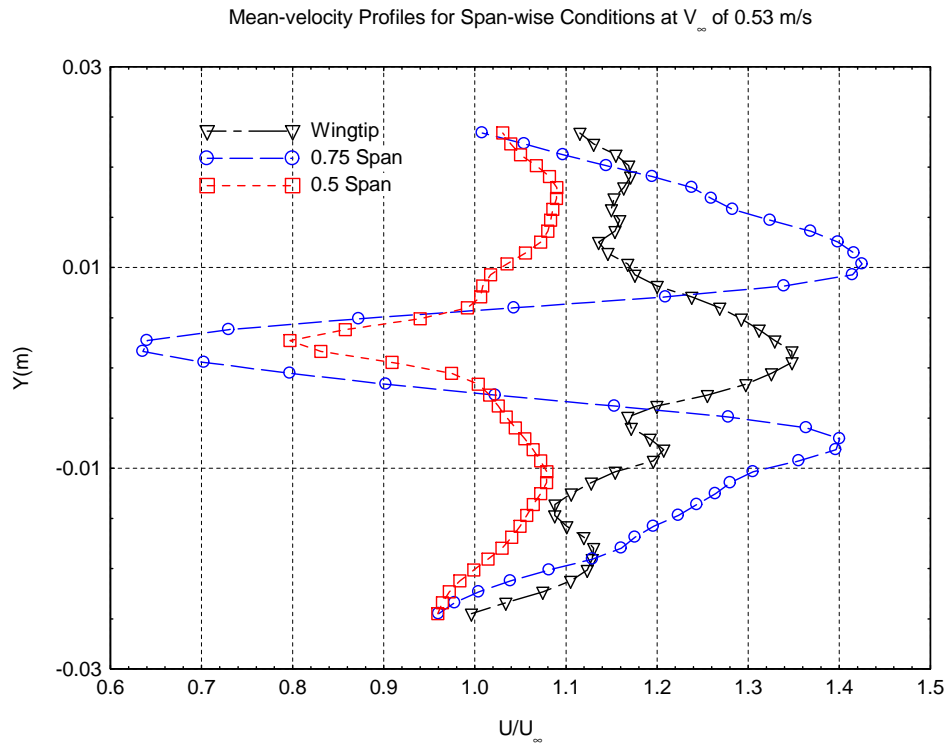
Figure 18. Mean Velocity Profiles for Varying Span-wise Location at V_∞=0.53m/s and V_∞=1.05m/s with an AoA of 0 Degrees

V∞ Effect

As V_∞ is increased the advance ratio of the flapping flight will increase. For the piezoelectric plate what is the relation between changing V_∞ (therefore J) and the vortex wake structures behind the flapping plate? How do the resulting wake structures from varying V_∞ to change J differ from those from varying the flapping amplitude to change J and what is the effect on the thrust generated by the flapping motion?

The voltage to the piezoelectric plate was kept constant during this experiment and the wind-tunnel motor speed was adjusted to increase the incoming flow condition. Despite the constant voltage, because of the aerodynamic forces on the plate as the wind-tunnel velocity increased, there was a significant drop in the amplitude of the flapping. Between the low speed and highest speed for V_∞ used in this study, about a 10 times increase in velocity, the amplitude was halved. This had the effect of more rapidly increasing the advance ratio with increasing V_∞ because of the corresponding drop in amplitude than would have otherwise been seen. There was still a significant difference in the amplitudes for any given J between the two cases with the V_∞ case consistently having larger h values over the amplitude effect case. The 0 degree angle of attack data was used to analyze the V_∞ effect and AoA was not considered in the comparison between V_∞ effect and amplitude effect. The mean-velocity information found in Figure 19 show that the jet like plumes found at J of 0.77 and 1.17 that provide a increase to the velocity magnitude and have a lower velocity region between the two jets match well with the corresponding J results from the amplitude effect results with the jets being stronger at similar J in the V_∞ case. At higher J values of 1.86 and 2.61 the plumes are no longer jet like because they have lower velocities then the

surrounding flow field. Instead, now between the two jets in the region that at the lower J

values had lower velocity than the plumes, a single high speed (higher velocity than V_∞) jet

appears about x/c=1.5 downstream from the trailing edge. This is in stark contrast to what

was seen in the amplitude effect mean velocities at the similar advance ratios of 1.68 and

2.78 where as is shown in Figure 11 they continue to have the jet like plumes going up and

down at an a slight angle away from the trailing edge of the flapping plate as was seen at

lower J. At J of 4.60 and 6.67 the mean-velocity shows agreement again with the amplitude

effect data where a single low speed wake is found directly behind the plate with no

diverging plumes. Another effect of the increased velocity can be seen in comparing the

mean velocity results at the leading edge of the plate. In general the V_∞ effect results show

some stagnation or decreased velocity magnitude regions at the leading and trailing edges

especially at the top and bottom of the piezoelectric plates flapping motion. The amplitude

effect results, in contrast, has no evidence of stagnation at the leading edge except for the

J=0.77 case. Figure 20 shows the plume angle of the Turbulent kinetic intensity can be seen

to increases with increasing J as it did for the amplitude effect case. Similar is that the

turbulence follows the vortex wake structure downstream and the regions of highest

turbulence are found directly behind the trailing edge with the exception of the high J cases

of 4.60 and 6.67. There is little turbulence downstream, as was the case with the high J

amplitude effect results, but now there are regions of high turbulence at the plate's location

with the highest regions being found at some of the leading and trailing edge locations at the

top or bottom of the flapping movement (phase angle of 90 or 270 degrees.) Vorticity

information for select cases is found in Figure 21. For J of 0.77 and 1.86 the amplitude is

again to large when compared to the image plane to determine what type of vortex structure

develops downstream from the plate. Looking at the vortex shedding for J=1.86 negative

vortices continue to form on the upper surface and positive on the lower surface. There

vortex formation continues to be at both leading and trailing edges as in the 0.77 J case but

now there is no separation along the chord of the plate until shedding occurs at the trailing

edge in the same manner. The J=4.6 case appears to have a von Kármán vortex sheet

forming downstream as a negative vortex over a positive can be seen at all four phase angles

while the shedding type is similar to the 1.86 J case. Looking at the mean-velocity profiles in

Figure 22 the velocity deficits are smaller than those found in the amplitude effect case for

similar J. In the varying amplitude case with the J=2.73 with an amplitude of A/c=0.6 and

V_∞ of 2.5 m/s has a force coefficient in the x direction ten times smaller than that for the

J=2.61 varying wind-tunnel velocity case with an amplitude of A/c=1.5 and V_∞ of 6.2 m/s.

As both cases have the same AoA and both vortex structures fit well into the PIV image

window this must be due to the differences in the vortex structure caused by the difference in

amplitude and V_∞. This difference is most apparent at lower advance ratios and can be seen

in Figure 23. These force coefficient values were found using the mean-velocity profiles at

two chord lengths downstream of the trailing edge and integrating the non-dimensional

velocity over the entire flow field. Because of the small size of the vortex structures at high J

values using the entire flow field causes the force coefficient to be more thrust like than it is

in reality which is why the force coefficient appears to be going to zero instead of dropping

into drag representative negative force coefficients.

Increasing V_∞ led to increasing J with the added effects of a drop in flapping

amplitude caused by the increased aerodynamic stresses on the flapping plate due to the

increased wind-tunnel flow velocity. The increased velocity causes turbulence to occur on

the piezoelectric plate especially on the leading and trailing edges. In comparing the amplitude effect to the V_∞ effect the following results stand out. Thrust generated by the piezoelectric flapping plate for a given J is highly dependant on flapping amplitude as smaller amplitudes lead to much smaller force coefficients in the x direction. The differences seen in the structure of the mean-velocities between the V_∞ effect and amplitude effect are of interest because they occur in the region of J where previous studies such as Lai and Platzer (1999) and Lua ET AL (2007) have shown that the change in vortex wake structures between going from thrust generating to neutral to drag generating occur, at J of about two to four. As shown in Lua ET AL (2007) and again here that amplitude plays a role in determining this as higher amplitudes generate more thrust at the same J (V_∞ changes) which leads to this assumption although the vortex structure in the present study is not visible for the J in this region due to the PIV image not showing downstream far enough from the piezoelectric plate. At higher flapping amplitudes the vortex structure tends to develop farther downstream.
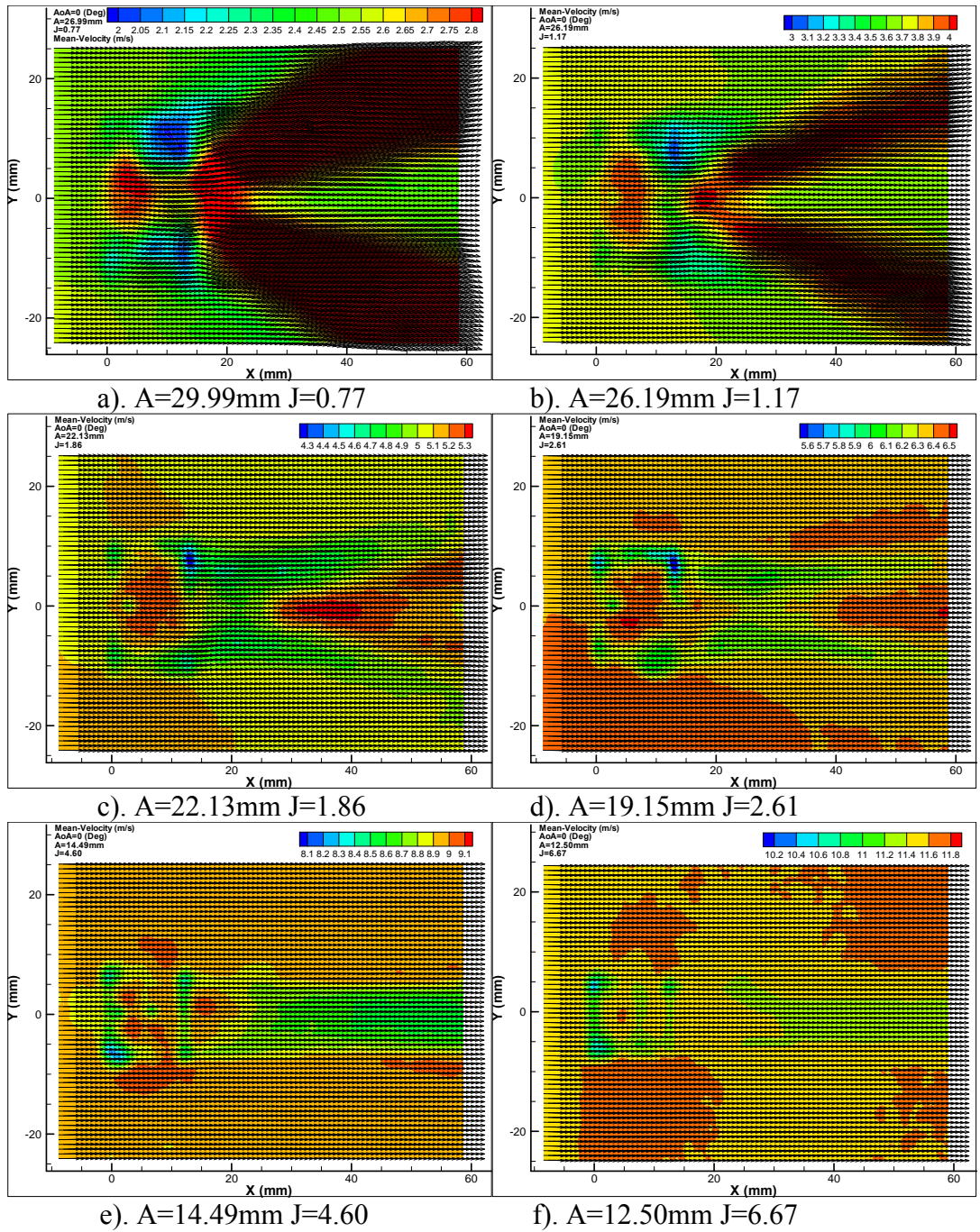
a). A=29.99mm J=0.77   b). A=26.19mm J=1.17

c). A=22.13mm J=1.86   d). A=19.15mm J=2.61

e). A=14.49mm J=4.60   f). A=12.50mm J=6.67

Figure 19. Mean-Velocity Magnitudes for Varying Incoming Flow Speed Data Set

a). A=29.99mm J=0.77

b). A=26.19mm J=1.17

c). A=22.13mm J=1.86

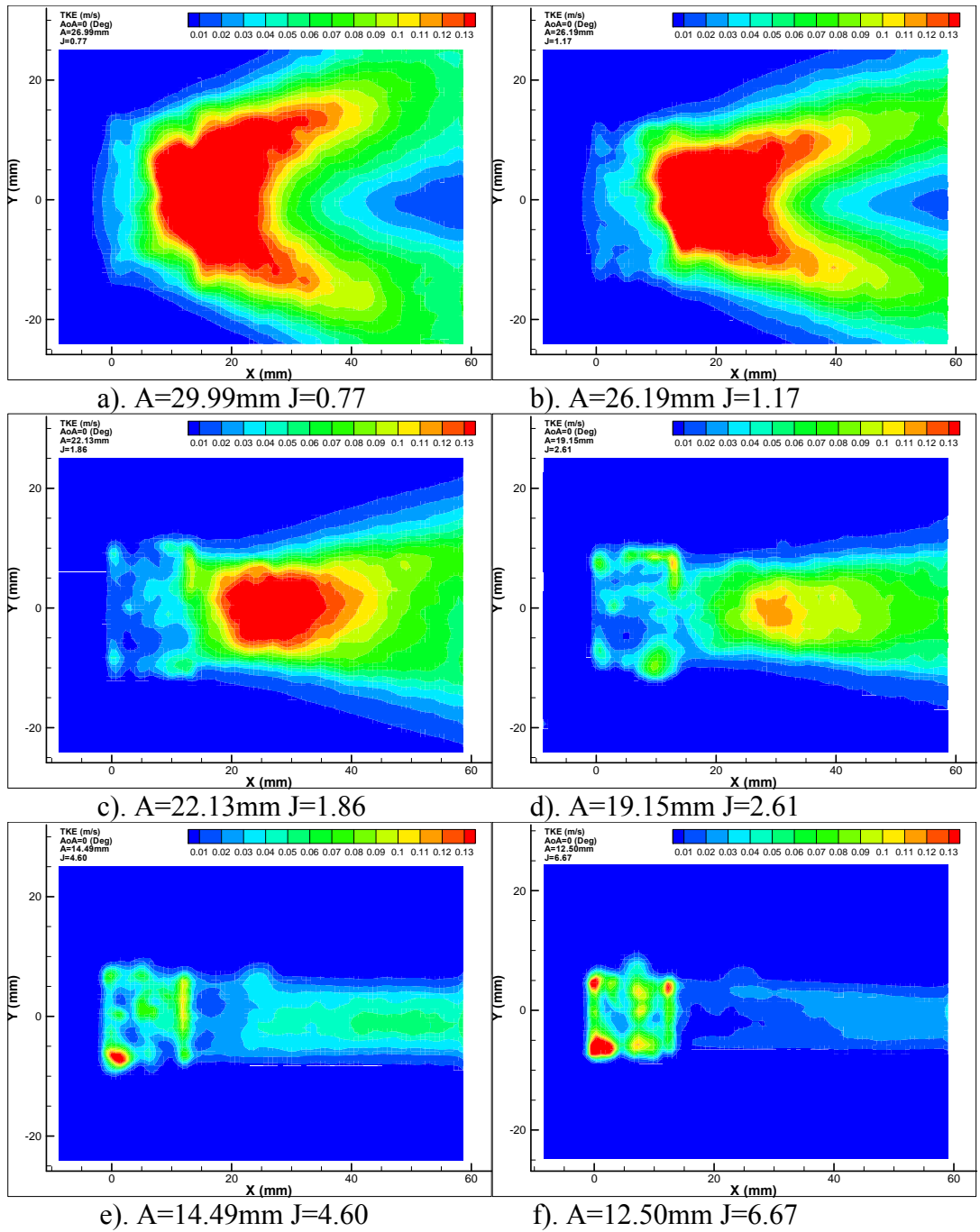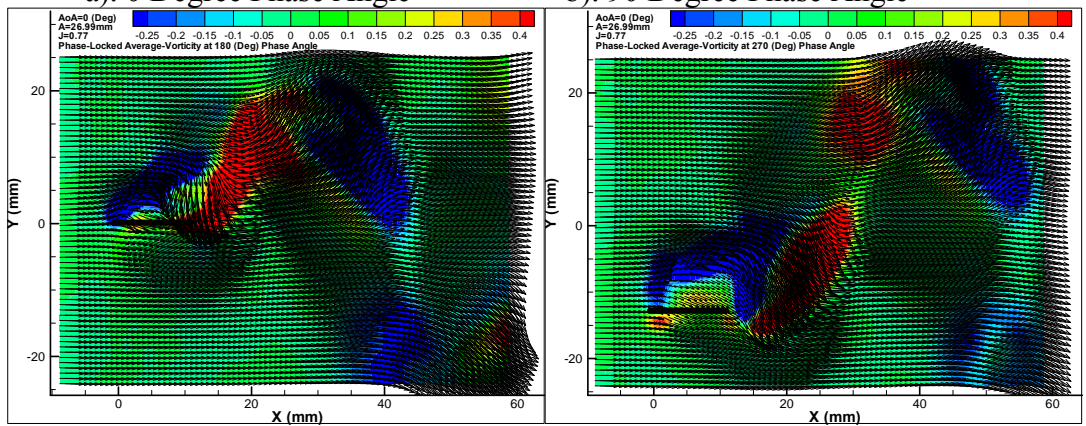d). A=19.15mm J=2.61

e). A=14.49mm J=4.60

f). A=12.50mm J=6.67

Figure 20. Turbulent Kinetic Energy of Varying Incoming Flow Speed Data Set
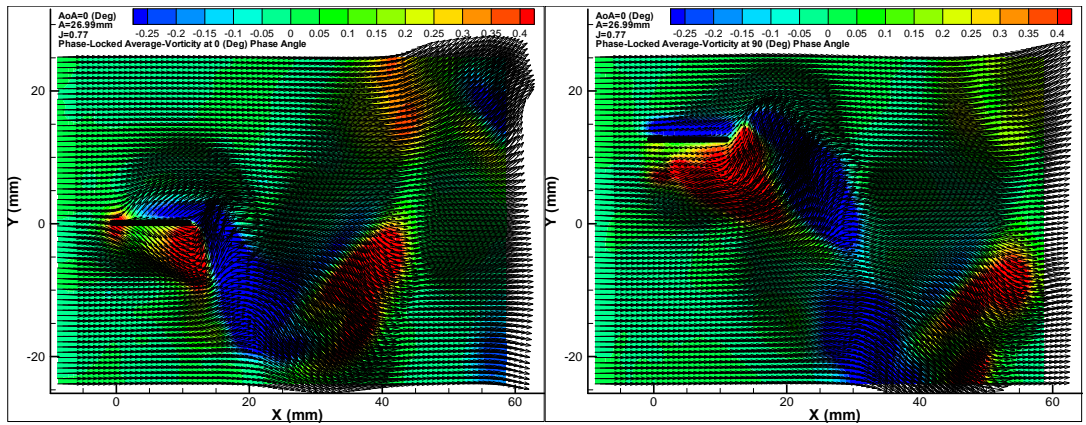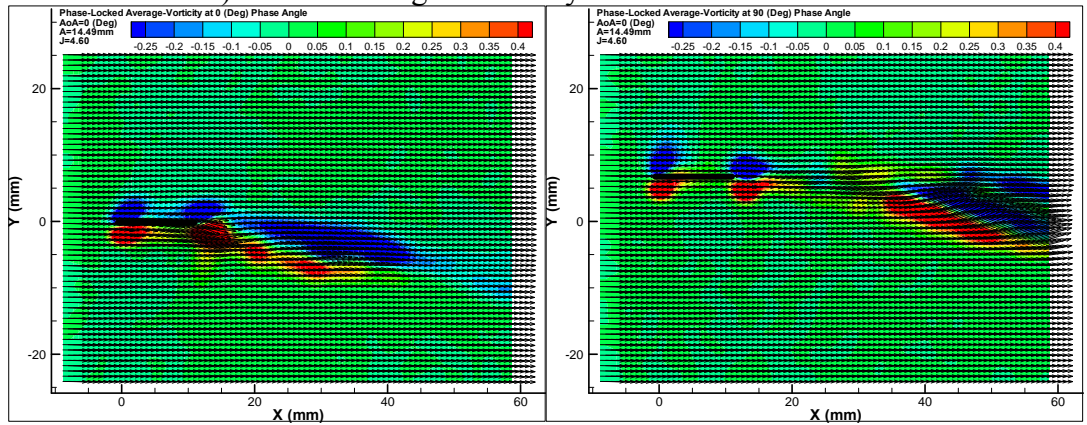
a). 0 Degree Phase Angle   b). 90 Degree Phase Angle

c). 180 Degree Phase Angle   d). 270 Degree Phase Angle

A). Phase-Averaged Vorticity for A=26.99mm J=0.77
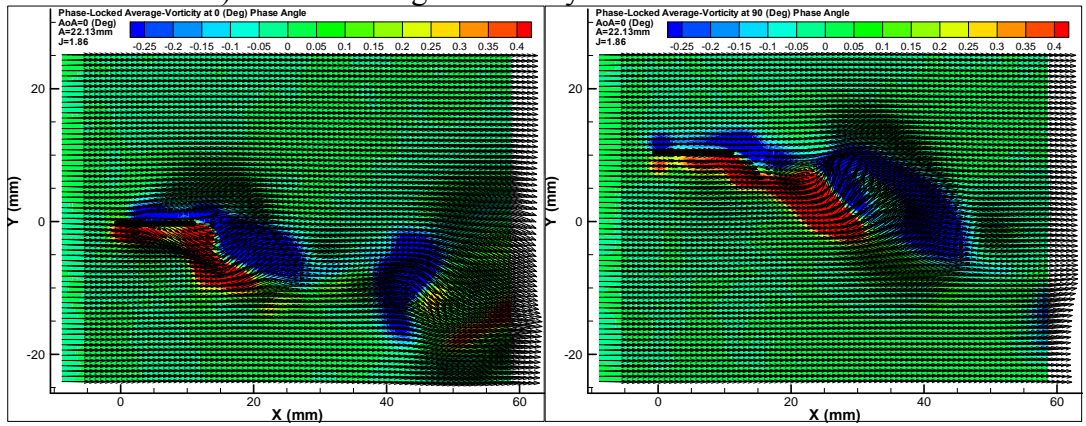
a). 0 Degree Phase Angle   b). 90 Degree Phase Angle
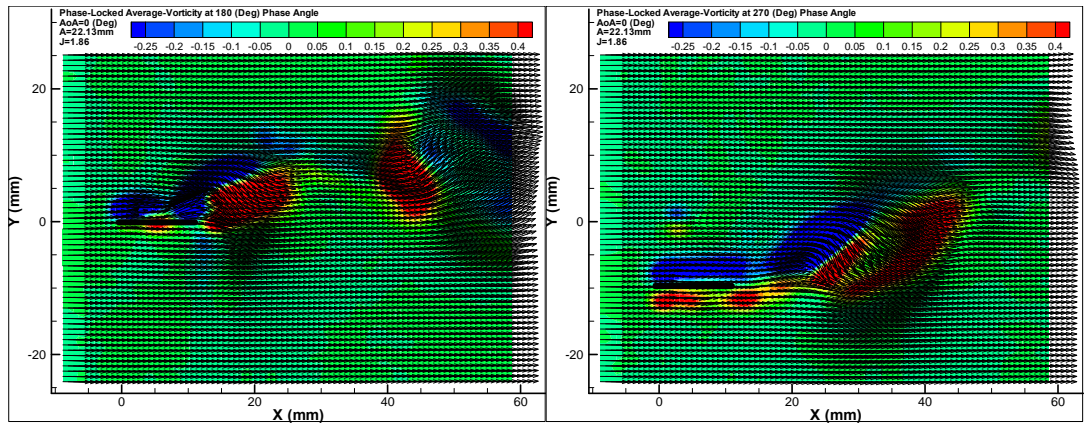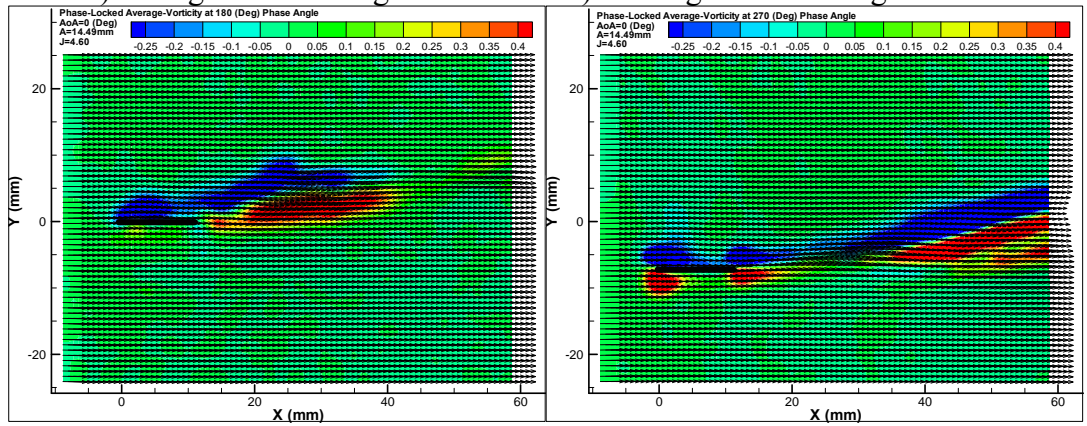
c). 180 Degree Phase Angle
d). 270 Degree Phase Angle

B). Phase-Averaged Vorticity for A=22.13mm J=1.86

a). 0 Degree Phase Angle
b). 90 Degree Phase Angle

c). 180 Degree Phase Angle
d). 270 Degree Phase Angle

C). Phase-Averaged Vorticity for A=14.49mm J=4.60

Figure 21. Phased-Averaged Vorticity at 0, 90, 180, and 270 degree Phase Angles for Select Varying Incoming Flow Speed Cases

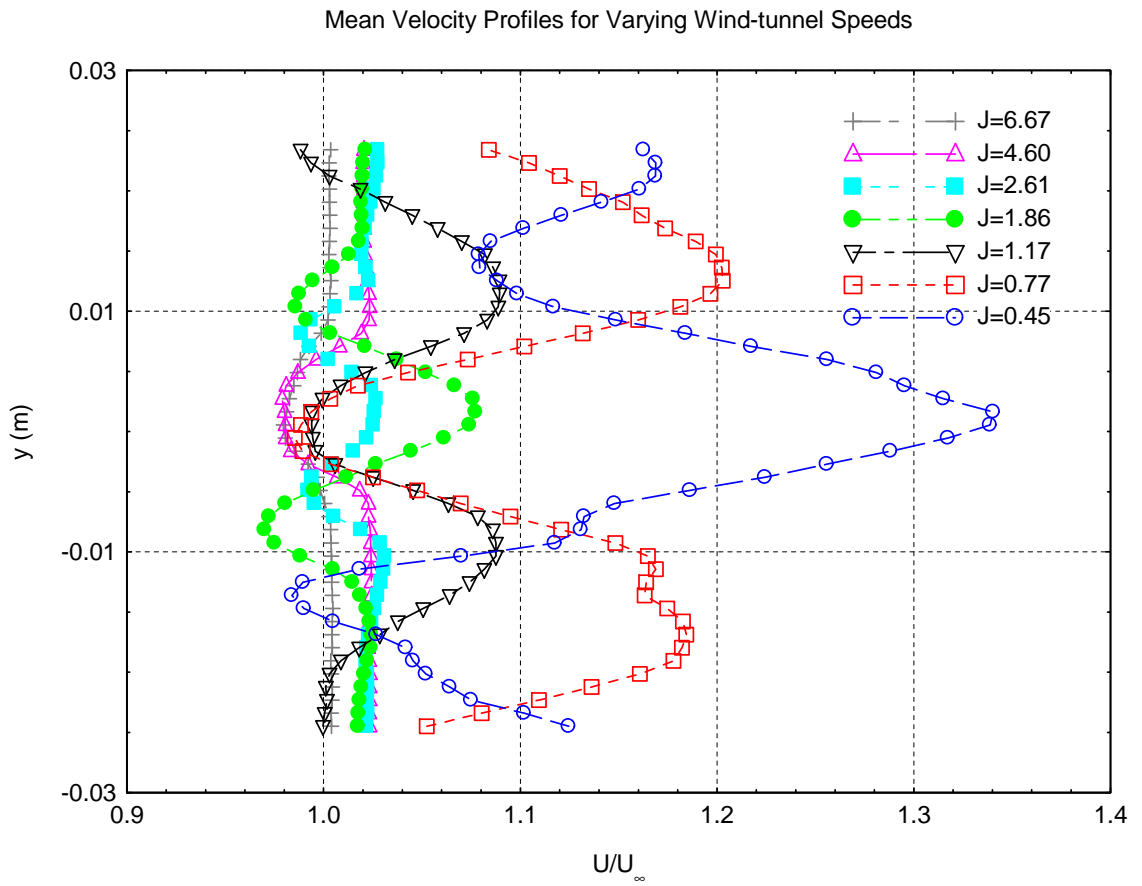Mean Velocity Profiles for Varying Wind-tunnel Speeds

Figure 22. Mean Velocity Profiles for Varying Wind-tunnel Speed Cases
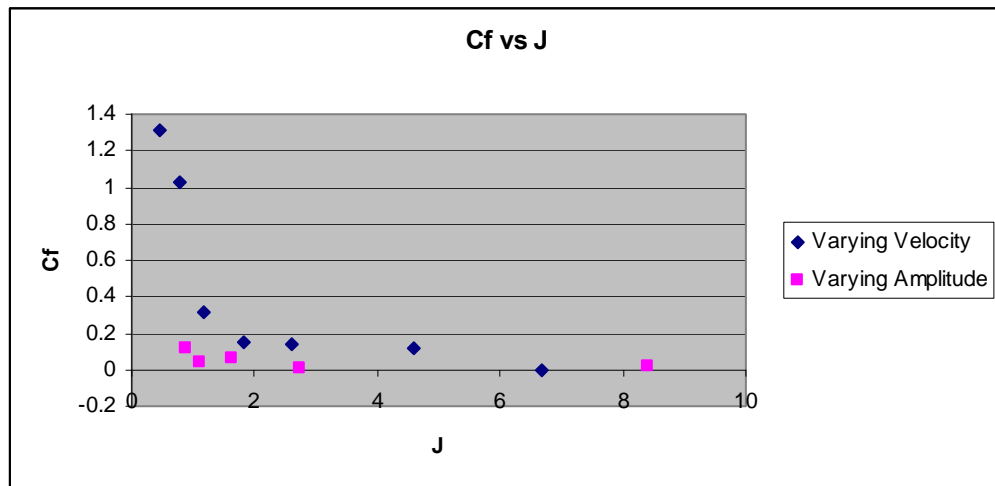

Figure 23. Comparison of the Force Coefficient in the x Direction by J for Varying Velocity and Amplitude Effect Cases

Angle of Attack Effect

As part of the larger V_∞ effect data set the AoA of the piezoelectric flapping plate was changed and PIV data gathered at the same conditions as those of the 0 AoA data. In looking at the AoA effect how does changing AoA influence the vortex structure, shedding, and thrust?

The effect of the AoA on the vortex structure is examined in Figure 24, Figure 25, Figure 26, and Figure 27 which cover AoA of 0, 10, and 20 degrees at wind-tunnel velocities of 2.5 and 11.55 m/s. Because of the increased aerodynamic forces on the plate at increased angle of attack the amplitude is lower at 20 degrees AoA than at 0 degrees AoA. This has caused small differences in the J value despite the same conditions in wind-tunnel velocity, power to the piezoelectric plate, and span-wise location. The mean-velocity magnitudes as seen in Figure 24 show that the increasing AoA has only slightly decreased the velocity magnitude and deflected the single drag wake directly behind the plate at high motor Hz but caused growing with increasing AoA low velocity regions on or near the flapping plate itself. At low motor Hz the two jet structure remains but is changed dramatically with increasing AoA. The jet structures have been deflected slightly, both downward with increasing AoA to a slightly lower position in y, but the greatest change is the rapidly decreasing with AoA velocity magnitude of the lower jet, so much so that it becomes much lower speed than the surrounding V_∞ flow by 20 degrees AoA. Due to the AoA and the deflection of the lower jet downward the lower jet at 20 degrees AoA follows directly behind the plate as a drag wake like structure. The AoA effect also increases the turbulent kinetic energy at the plate location and in the lower jet structure with increasing AoA as shown in Figure 25. At the 3 Hz wind-

tunnel speed the turbulence is seen to greatly increase with increasing AoA both at the

piezoelectric plate location and in the wake. At 10 Hz the turbulence is more similar at the

plate location for the different AoA but with increasing AoA the upper jet becomes less and

the lower jet more turbulent. Looking at the vortex shedding, because the large amplitudes

make low J vortex structures develop too far downstream, the effect of changing AoA can be

seen in Figure 26. There is little difference in the shedding type by AoA but the separation

bubble of detached and reattaching flow on the negative vortex generating lower side of the

plate can be seen at a phase angle of 90 degrees to increase in size with AoA just as the

separation bubble on the upper positive vortex generating side of the plate seen at a 180

degree phase angle is decreasing with increasing AoA. The most evident effect of increasing

AoA is increased drag which can be seen from the mean-velocity profiles in Figure 27. The

images are for positive AoA and thus flipped from the PIV data but it is clear from the 3 Hz

plot that the increasing AoA greatly increases the drag as well as how the wake structure

goes from symmetric at 0 AoA to at the 20 AoA profile showing a large drag wake behind

the plate with a slightly smaller jet like structure above than was found at the 0 AoA. At the

10 Hz high wind-tunnel speed wake profile the single wake structure leads to a simpler

increased drag wake with increasing AoA result. In Table 10 the conditions of the cases

presented in the AoA effect section are given along with the calculated force coefficient in

the x direction found from the mean-velocity profiles from Figure 27. Increasing the AoA to

20 degrees, even for a case with the advance ratio below one, completely eliminates the

thrust advantages from flapping. Again the entire image was used to calculate the force

coefficient, so at the low J values because of the large size of the vortex structures compared

to that of the PIV image not all the information is available, while at the large J values the

small size of the wake structure this method tends to increase the force coefficient.

Table 10. Varying AoA Data Set Cases for Wind-tunnel Motor 3 and 10 Hz by AoA, A, h, k, kh, Strouhal, J, Re, and Force Coefficient in the x Direction

Motor (Hz)	AoA (Deg)	A (m)	h	k	kh	Strouhal	J	Re	Cf in x
3	0	0.027	1.063	0.974	1.035	0.325	0.77	2064.8	1.031
3	10	0.027	1.063	0.974	1.035	0.325	0.77	2064.8	0.057
3	20	0.026	1.016	0.974	0.989	0.309	0.81	2064.8	-0.265
10	0	0.013	0.492	0.239	0.118	0.037	6.67	8401.5	-0.007
10	10	0.011	0.436	0.239	0.104	0.033	7.53	8401.5	-0.082
10	20	0.010	0.387	0.239	0.093	0.029	8.48	8401.5	-0.125

The results of changing AoA at low J was deflected Jet like mean-velocity structures

with the jet behind the flapping plate at higher AoA becoming a low velocity wake. The

vortex shedding between AoA was very similar with separation bubbles becoming larger

with higher AoA. It is hypothesized that with higher AoA at some AoA above 20 the leading

edge separation will not reattach. For the AoA tested in the current study this was not seen.

Increasing AoA was found to greatly reducing the benefit to thrust from flapping and by 20

degrees AoA even at the lowest advance ratios examined the thrust benefits became

negligible.

a). AoA=0 (Deg) at 10 Hz Motor Speed   b). AoA=10 (Deg) at 10 Hz Motor Speed

c). AoA=20 (Deg) at 10 Hz Motor Speed   d). AoA=0 (Deg) at 3 Hz Motor Speed

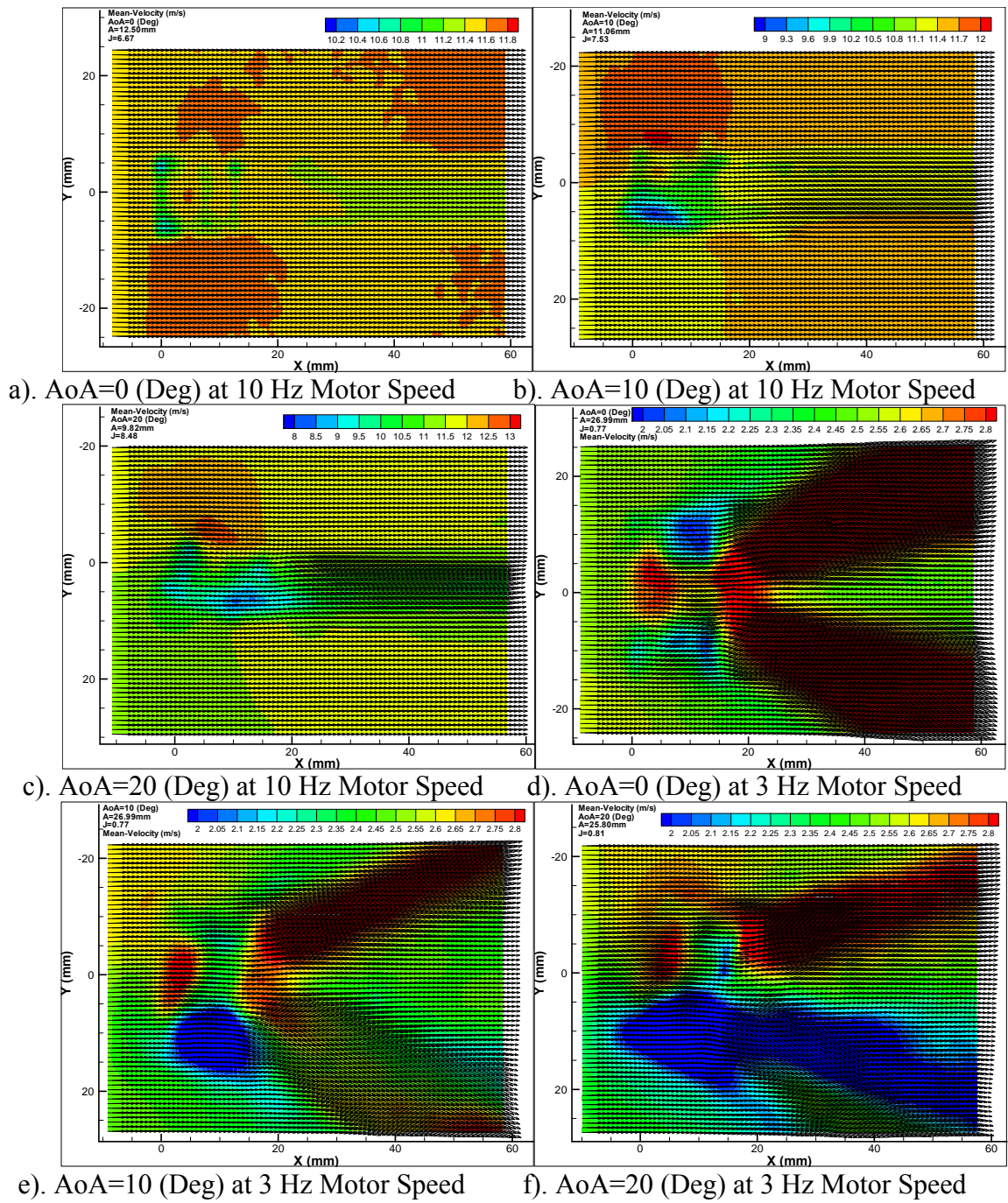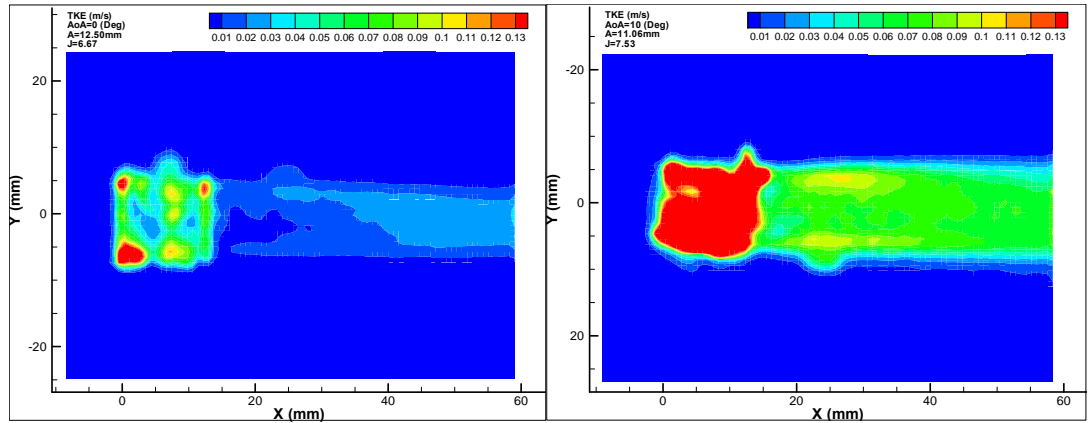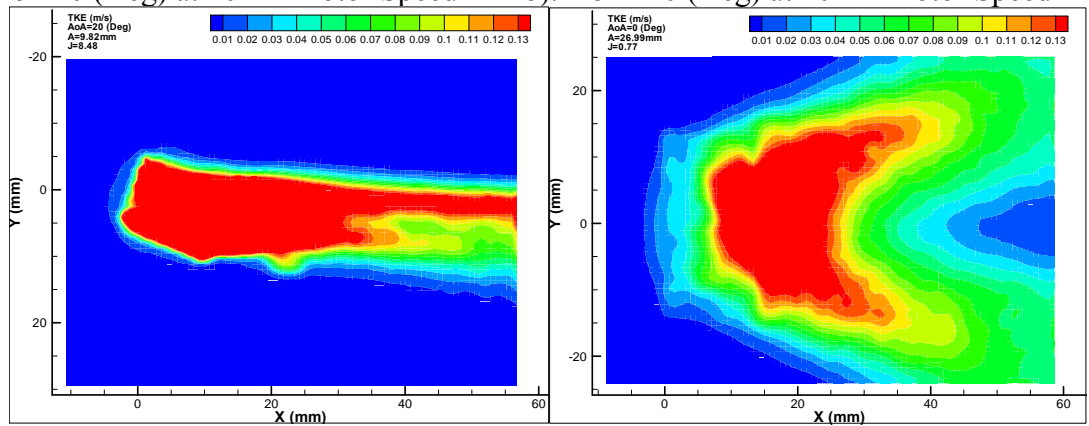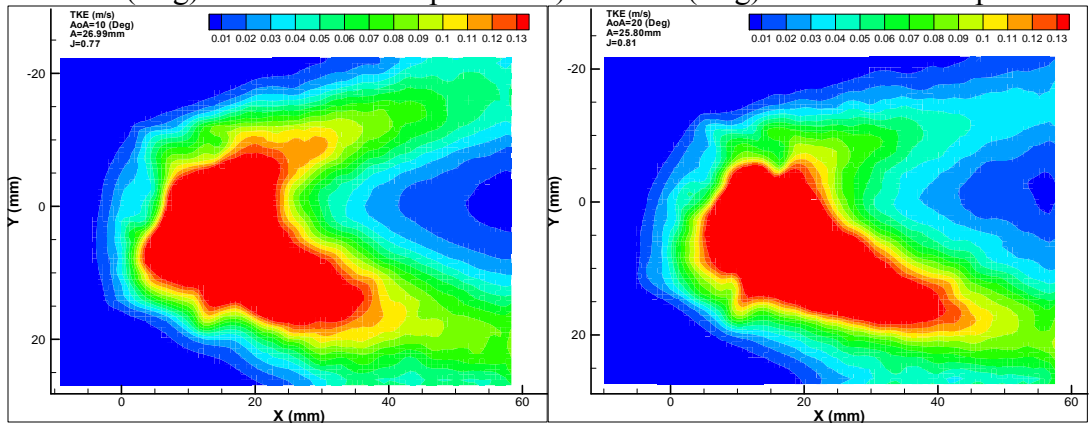e). AoA=10 (Deg) at 3 Hz Motor Speed   f). AoA=20 (Deg) at 3 Hz Motor Speed

Figure 24. Mean-Velocity Magnitudes at 0, 10, and 20 degree AoA at 3 Hz and 10 Hz Wind-tunnel Motor Speeds

a). AoA=0 (Deg) at 10 Hz Motor Speed   b). AoA=10 (Deg) at 10 Hz Motor Speed

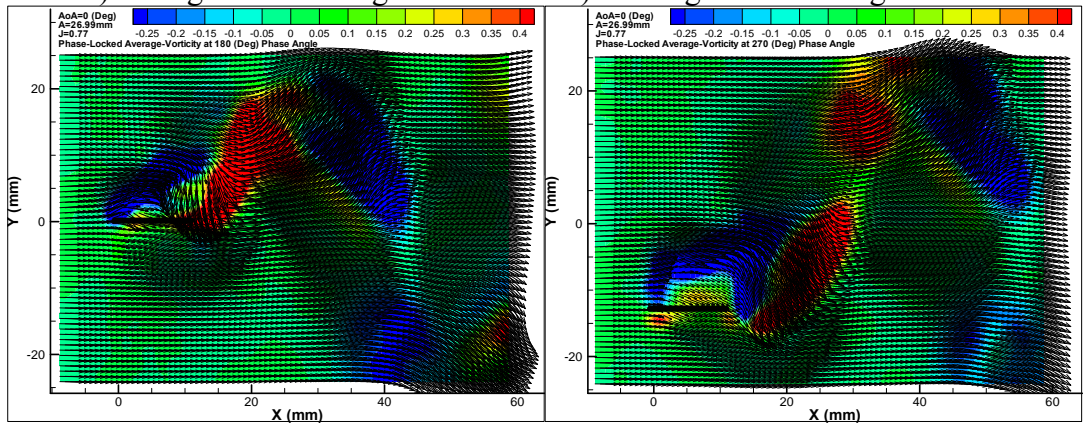c). AoA=20 (Deg) at 10 Hz Motor Speed   d). AoA=0 (Deg) at 3 Hz Motor Speed

e). AoA=10 (Deg) at 3 Hz Motor Speed   f). AoA=20 (Deg) at 3 Hz Motor Speed

Figure 25. Turbulent Kinetic Energy at 0, 10, and 20 degree AoA at 3 Hz and 10 Hz Wind-tunnel Motor Speed
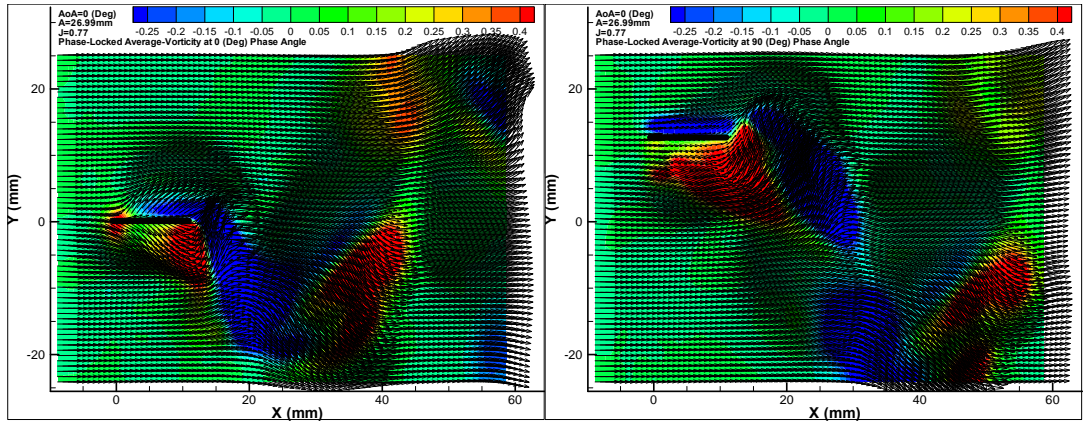
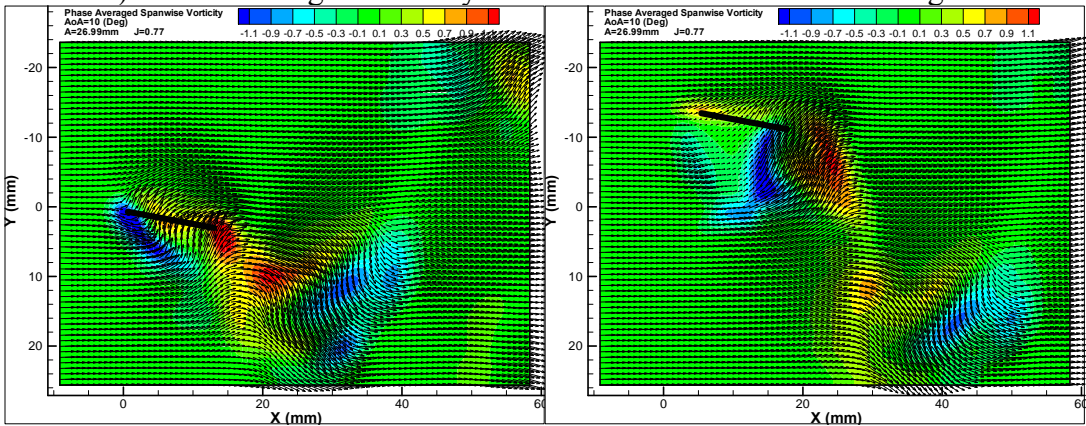a). 0 Degree Phase Angle   b). 90 Degree Phase Angle
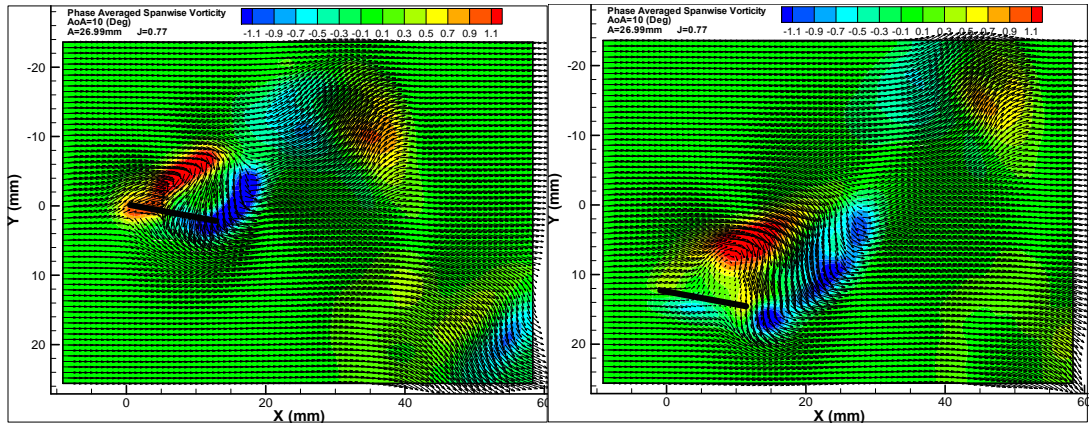
c). 180 Degree Phase Angle   d). 270 Degree Phase Angle

A). Phase-Averaged Vorticity for A=26.99mm J=0.77 AoA 0 Degrees
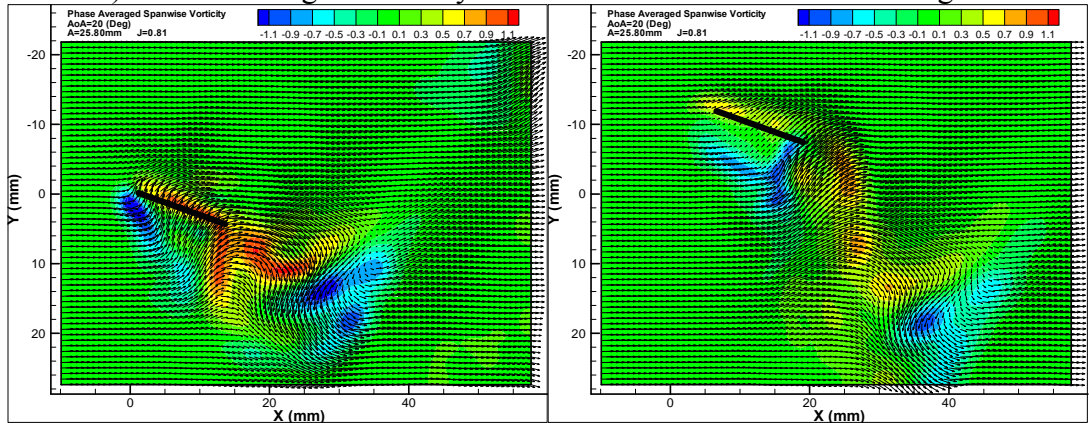
a). 0 Degree Phase Angle   b). 90 Degree Phase Angle
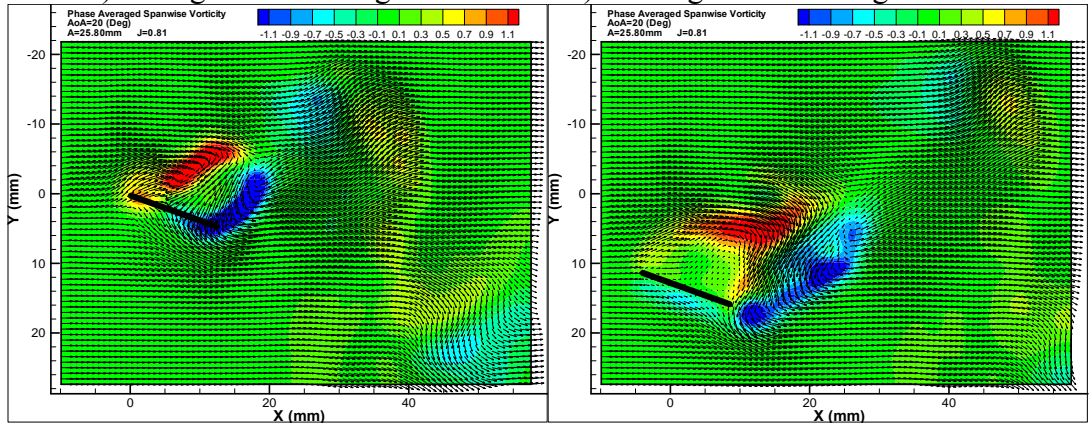
c). 180 Degree Phase Angle   d). 270 Degree Phase Angle

B). Phase-Averaged Vorticity for A=26.99mm J=0.77 AoA 10 Degrees

a). 0 Degree Phase Angle   b). 90 Degree Phase Angle

c). 180 Degree Phase Angle   d). 270 Degree Phase Angle

C). Phase-Averaged Vorticity for A=25.80mm J=0.81 AoA 20 Degrees

Figure 26. Phased-Averaged Vorticity at 0, 90, 180, and 270 degree Phase Angles for Varying AoA Conditions at 3 Hz Wind-tunnel Motor Speed
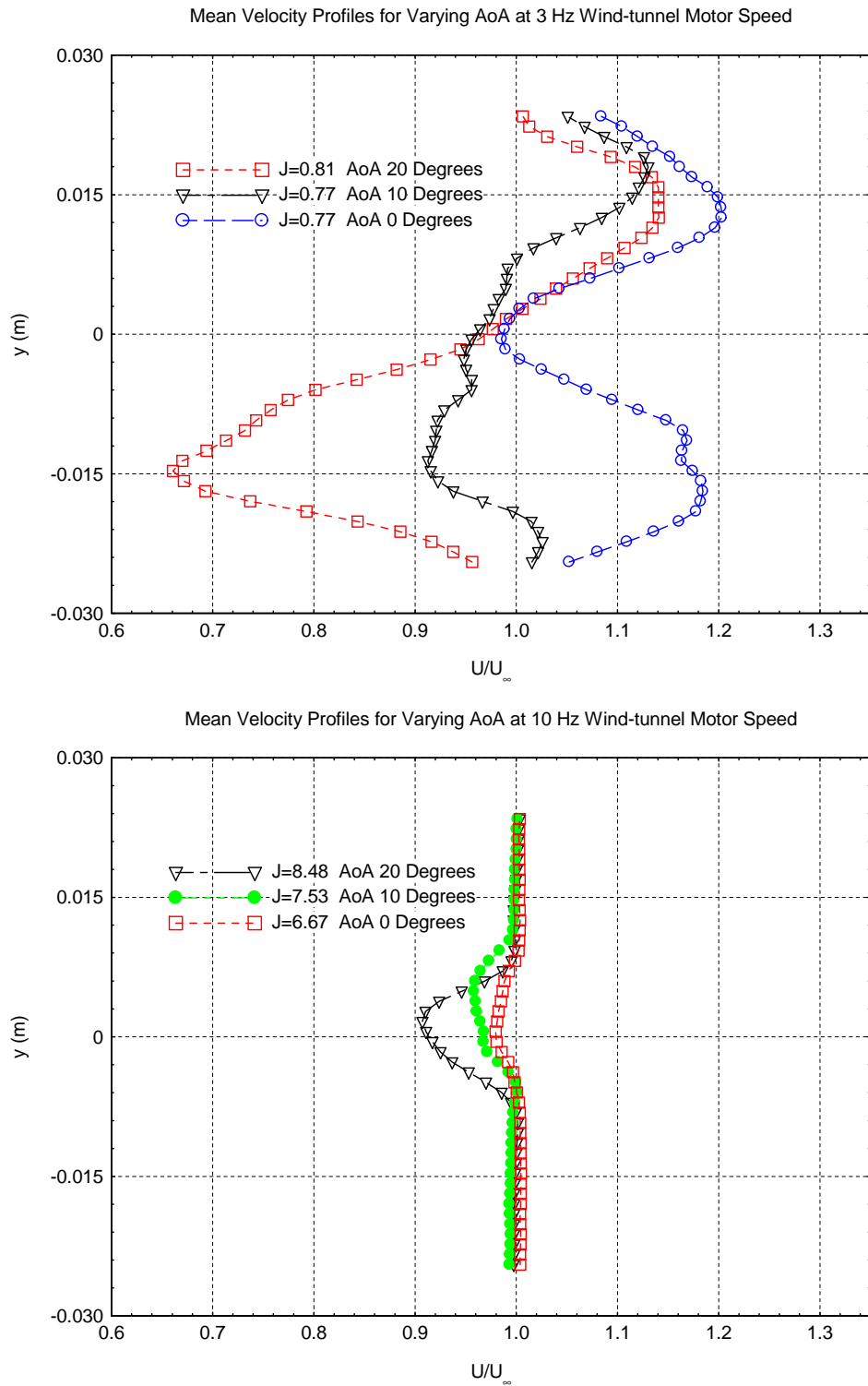
Mean Velocity Profiles for Varying AoA at 3 Hz Wind-tunnel Motor Speed

Mean Velocity Profiles for Varying AoA at 10 Hz Wind-tunnel Motor Speed

Figure 27. Mean Velocity Profiles for Varying AoA for 3 Hz and 10 Hz Wind-tunnel Motor Speed

CHAPTER 5. SUMMARY AND DISCUSSION

Conclusions

In the present study the effects of changing advance ratio, angle of attack, flapping amplitude, and span-wise location on the flow structures in the wake of a piezoelectric flapping plate was explored. It was shown from the wake profiles, as shown in previous studies (such as Lai and Platzer (1999)), that at low advance ratios, close to and less than one, generate jet like thrust generating vortex structures. As the advance ratio is increased, keeping constant amplitude and frequency of flapping, the wake structure becomes neutral and then drag generating. The trend of thrust generation related to changing J was confirmed by the force measurements of Hu ET AL (2008), where for advance ratios less than one they found a large increase in the thrust generated and as J increased from one the thrust benefit from flapping dropped off. Therefore at low flight speeds (low Reynolds numbers, such as in NAV applications) with high flapping frequency and amplitude flapping flight is more efficient in the thrust generated. As the flight speed increases (increasing J) the thrust benefit gained from flapping diminishes to the point that eventually the flapping causes increased drag. As was discussed in previous studies, such as Lai and Platzer (1999), this effect is not alone dependent on J and can vary with amplitude and frequency of flapping. Varying the amplitude or the wind-tunnel velocity to adjust the advance ratio results in different values of k and h for similar J values and has some effect on the vortex structure. From a common minimum velocity and maximum amplitude, varying J by increasing the V_∞ and separately by decreasing the amplitude leads to more drag at similar J when the amplitude is smaller.

The AoA was shown to deflect the wake structure, change the velocity profiles dramatically at low J values, increase drag at higher angles of attack, and to increase the size of separation bubbles found at low J values. The wake structure type was not found to be AoA dependant for the AoA used in the study. The span-wise location proved to be important to the wake structure at low J values as very distinct different wake structures were seen along the span at the same V_∞ conditions. These differences were not able to be identified as due only to the change in amplitude resultant from the span-wise location. The jet like properties of the wake structure seen at low advance ratios decreases as the span-wise measurement location moves inward from the wingtip. Also, when comparing similar cases of advance ratio and flapping amplitude between wingtip and a span-wise location, the resulting vortex structures can be different. Understanding the cause of this phenomenon requires further study.

Recommendations for Future Work

A camera lens enabling a wider field of view would enable the vortex structures caused by the larger flapping amplitudes the piezoelectric plate is capable of to be better measured and identified.

Due to the importance of span-wise location to the vortex structure a better understanding of how this change occurs would be very useful. As the piezoelectric plate is three dimensional, by employing the Stereoscopic Particle Image Velocimetry technique the span-wise vortex structure would be better reveled by the three dimensional measurements allowing for a better understanding of the vortex structures in the wake of flapping airfoils.

The piezoelectric plate is well suited to continuing the work on dragonfly flight physics by using two in tandem to study the effect of the vortex wake structure on the second airfoil downstream in the wake of the first and the interactions of merging vortex sheets.

Varying the piezoelectric plate parameters such as span, frequency, and chord length to confirm the results are for any flat plate flapping airfoil or to show how structure is dependant on airfoil size would help further this study.

62

REFERENCES

Bohl, D. G. and Koochesfahni, M. M., "MTV measurements of the vertical field in the wake of an airfoil oscillation at high reduced frequency," *Journal Fluid Mechanics*, Vol. 620, 2009, pp. 63-88.

Hu, H., Kumar, A. G., Abate, G., and Albertani, R., "An Experimental Study of Flexible Membrane Wings in Flapping Flight," AIAA-2009-0876.

Lai, J. C. S. and Platzer, M. F., "Jet Characteristics of a Plunging Airfoil," *AIAA Journal*, Vol. 37, No. 12, 1999, pp. 1529-1537.

Lua, K. B., Lim, T. T., Yeo, K. S., and Oo, G. Y., "Wake-Structure Formation of a Heaving Two-Dimensional Elliptic Airfoil," *AIAA Journal*, Vol. 45, No. 7, 2007, pp. 1571-1583.

Murphy, J. T., "Experimental investigation of biomimetic wing configurations for Micro Air Vehicle applications," Thesis, Aerospace Engineering Department, Iowa State University, Ames, IA, 2008.

Platzer, M. F., Jones, K. D., Young, J., and Lai, J. C. S., "Flapping-Wing Aerodynamics: Progress and Challenges," *AIAA Journal*, Vol. 46, No. 9, 2008, pp. 2136-2149.

Young, J., "Numerical Simulation of the Unsteady Aerodynamics of Flapping Airfoils," Thesis, School of Aerospace, Civil and Mechanical Engineering, The University of New South Wales, Australian Defence Force Academy, 2005.

Young, J. and Lai, J. C. S., "Oscillation Frequency and Amplitude Effects on the Wake of a Plunging Airfoil," *AIAA Journal*, Vol. 42, No. 10, 2004, pp. 2042-2052.

ACKNOWLEDGEMENTS